The Blackfoot III buried geophone experiment

Dan Cieslewicz and Don C. Lawton

ABSTRACT

The Blackfoot III buried geophone experiment was composed of three 3-component receiver lines buried to depths of 6, 12 and 18 meters, and one at the surface, occupying the central kilometer of a three kilometer shot line. The vertical channel data quality was found to be similar for all geophone depths, while the radial channel data was found to have highest quality at the surface and poorest for the buried phones. Data from buried geophones were affected by mode leakage, which adversely affected the data quality. The bandwidths of the P-P and P-S reflections were not consistent between the different geophone depths and between stations, indicating that geophone coupling was likely the dominant factor in recorded frequency. Because of this, the frequency analysis indicated no systematic compressional- or shear-wave attenuation through the overburden layer. Higher P-wave interval velocities suggested a thinning of the overburden layer at the eastern third of the line, which corresponds to an increase in surface elevation. The S-wave velocities were not similarly affected. Quantitative calculations of similarity between the processed sections revealed that random noise was the dominant factor controlling the absolute similarities between sections, as any factor that reduced random noise tended to make the sections more similar. Apart from this, sections that were closer in relative depth tended to be more alike, perhaps due to similar receiver notch patterns. Sections from shallower depths also tended to be more similar than sections from deeper depths, perhaps as a result of increased reflection amplitude in shallower phones causing better signal-to-noise ratios. The effect was not as clear for the converted-wave data. On the vertical channel data, the Glauconite valley-fill sandstone appeared as a high-amplitude trough that broadened and decreased in amplitude toward the off-channel lithologies. The overlying coal markers changed from a single peak to a doublet, possibly a compaction-related effect. The radial channel seismic expression of the producing unit was similar, though not as pronounced. Overall, burying geophones does not appear to be a viable way of improving converted-wave bandwidth or determining attenuation constants of the near surface.

INTRODUCTION

In October, 1997, CREWES conducted the Blackfoot III seismic survey, which tested and compared different seismic acquisition methods over a known oil-producing formation. Variables included receiver spacing, receiver depths, geophone types, source sizes and source depths, with the overall goal of determining the combination that would best image the reservoir. This paper details the effect of varying receiver depth on seismic data. The survey was designed to make it possible to produce compressional- and converted-wave stacked sections from receiver lines at depths of 0, 6, 12 and 18 meters below surface. The raw and processed data from each depth were analyzed and compared to evaluate the effect of geophone depth on seismic data noise levels, bandwidth, and other factors. This experiment is essentially a much larger version of the buried geophone experiment conducted by CREWES last year in southern Alberta (Cieslewicz and Lawton, 1997), though the results from that experiment were likely influenced by a very thick overburden layer.

Converted-wave data from buried geophones might be expected to have a broader bandwidth than data from surface geophones. Bandwidth comparisons of surface and VSP data (e.g. Zhang *et al.*, 1994) demonstrate that converted waves undergo substantial attenuation between bedrock and the surface. Since an important difference between a VSP and a surface survey is the presence of the near-surface layer, it is possible that the near-surface layer is responsible for attenuating converted waves. Laboratory measurements indicate that unconsolidated overburden can be very attenuative to shear waves (Kudo and Shima, 1970). By avoiding a portion of the near surface, therefore, a buried geophone may avoid some amount of attenuation.

Due to the unique receiver geometry, high-resolution interval velocities of the overburden layer can also be determined with the buried geophone data. This will enable us to better understand the seismic characteristics of the near surface, which has an important but often underappreciated effect on seismic data quality and, ultimately, the interpretation of the deeper reflections.

The buried receiver lines are only several meters apart in relative depth, and all have a common source, so the data can also be used as a test of seismic survey repeatability, as each line samples essentially the same wave field. Several statistical comparison techniques are used to determine the similarity of data between the buried lines, and distinguish effects of burial from effects of non-repeatability. We also present a brief interpretation of the vertical and radial channel data.

LOCATION

The Blackfoot field is located in Township 23, Range 23W4, about 45 kilometeres southeast of Calgary, Alberta. It produces oil from porous, channel-fill sediments of the Lower Cretaceous Glauconite Member of the Mannville formation.

GEOMETRY AND ACQUISITION

The shot line was three kilometers long and oriented nearly E-W (Figure 1). The source was 4 kg of dynamite detonated at 18m depth, at a nominal shot spacing of 20m. The receivers were OYO three-component geophones. Prior to the survey, the geophones were coupled with high-strength aircraft cable threaded through the casing, so that they could be winched out of the holes after the survey. A sand spike was affixed to the geophone by threading the cable through it (Figure 2). The sand spike, because it protrudes from the bottom, was intended to prevent the geophone from turning sideways in the hole during emplacement or extraction, which may damage it.

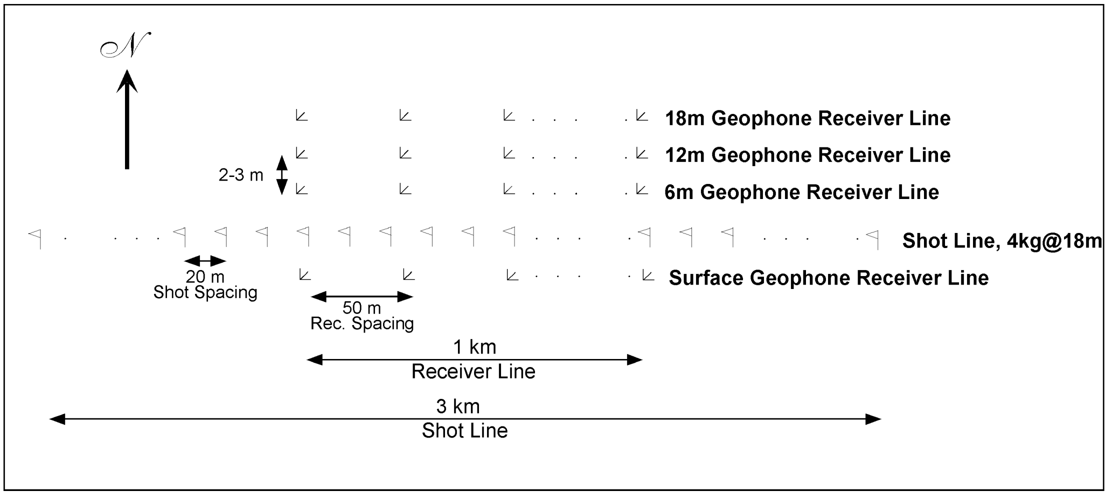

Figure 1. Buried geophone experiment survey geometry.

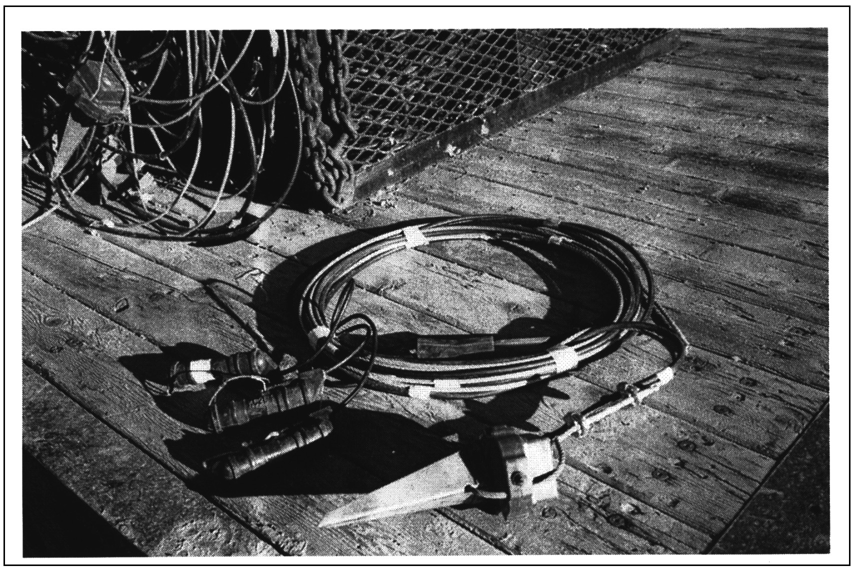

Figure 2. Geophones in the experiment were fitted with sand spikes for stability during emplacement and extraction, and aircraft cable to assist in their recovery.

Twenty-one buried geophone stations occupied the central kilometer of the shot line, at a spacing of 50m. At each station, a shot hole rig augured three holes to approximately 6, 12 and 18m depth. The modified geophones were affixed to the end of a wooden planting pole and lowered down each hole. Pole planters encountered varying amounts of thick mud before obtaining a firm plant. In many cases, the geophones could not be placed at the desired depth due to borehole infilling and obstructions, or because the augur could not drill a deep enough hole due to bedrock or boulders. At three stations, the 18m phone could not even be placed as deeply as the 12m phone. For simplicity, each geophone level will be referred to as 6m, 12m and 18m, even though not every geophone attained the desired depth. Figure 3 shows the actual geophone depths for each station.

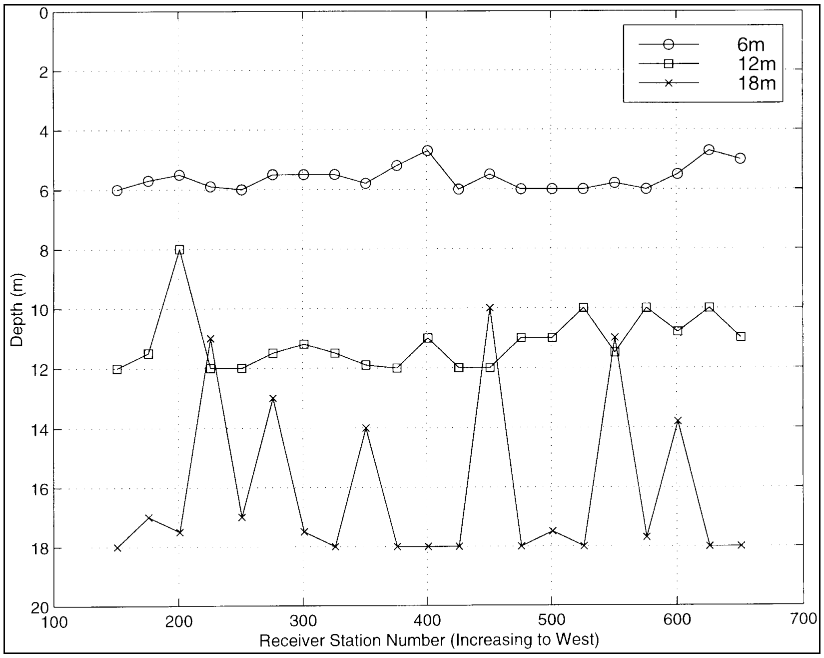

Figure 3. Actual buried geophone depths below surface. Geophones could not always be placed at the desired depth due to borehole obstructions.

Geophones were also hand-planted, leveled and aligned on the surface in the usual fashion. The geophones were live for all shots, and recorded six seconds of data at a one millisecond sample rate.

PROCESSING

All data for the buried geophone experiment were processed in Promax. The survey geometry resulted in a maximum fold of 65 (Figure 4a) for the vertical channel section, and 76 for the radial channel section (Figure 4b). The first 2.5 seconds of data were processed, which contained the zone of interest, and was sufficient to tie in the longest synthetic traces for later interpretation.

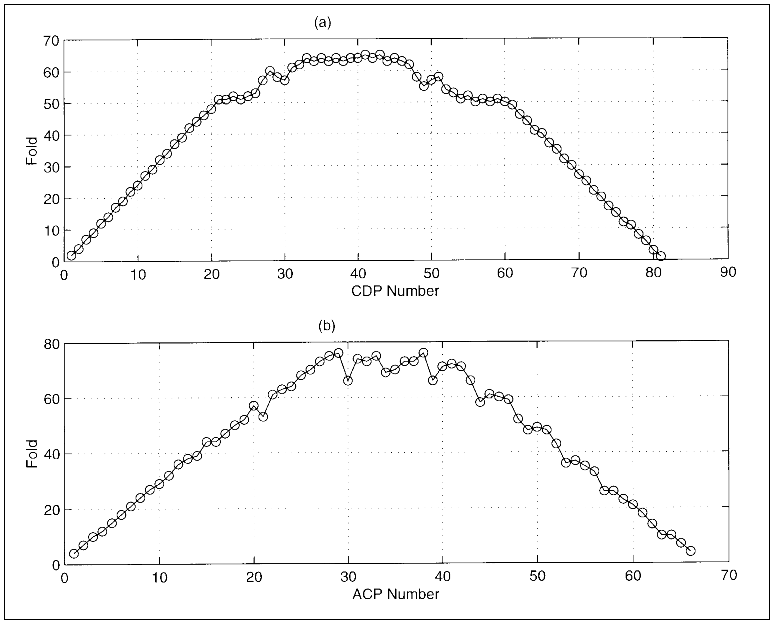

Figure 4. (a) Vertical channel fold. (b) Radial channel fold.

Vertical Channel

The vertical channel data were binned to a 25 meter CDP spacing, and processed to preserve relative amplitudes within each section. The processing flow was identical for surface and buried receiver data, with the exception that the buried geophone data required receiver kills. An independent residual statics calculation was made for each geophone level, as receiver statics would obviously be different.

The main processing steps for the vertical channel data included:

Assign geometry

Surface-consistent deconvolution

True amplitude recovery
4db/sec gain and correct for geometric spreading

Time-variant spectral whitening
Balance frequencies between 6 and 130 Hertz

Elevation statics
Calculated using elevations and uphole shot times

Velocity Analysis

Residual statics
Apply correlation autostatics

NMO correction
No stretch mute

Top mute

Time-variant scaling

CDP stack

15% Alpha-trim mean

Bandpass filter

8-12-100-120 Hertz zero phase Ormsby

Trace equalization

Migration

Phase shift time migration @ 90% stacking velocities

The fully processed sections for the vertical channel appear in Figures 5-8. The quality of data from the four different depths is similar.

Horizontal Channels

In general, the converted-wave data from all geophone depths had lower signal-to-noise ratios, reduced bandwidth and larger receiver statics compared to the compressional-wave data. These observations are usual for multi-component seismic surveys (e.g. Zhang *et al.*, 1994). The buried geophones were affected by additional problems of polarity reversals and mode leakage, which were not observed in the surface data. These are acquisition-related problems caused by a tendency for geophones to twist out of alignment with the shot line and tilt away from vertical during planting, which would respectively result in converted-wave reflections on the transverse channel and compressional-wave reflections on one or both of the horizontal channels. It is also possible that the converted- and compressional-wave reflections are not yet refracted to parallel, vertical raypaths at the depth of the buried phones, resulting in mode leakage. In many instances, converted-wave reflections had approximately equal amplitude on both the radial and transverse channels.

Because of these and other factors, the horizontal channel data required several additional processing steps and specialized processing techniques not required for the vertical channel data. Descriptions of these special considerations follow in the next sections. Important processing steps for the horizontal channel data were:

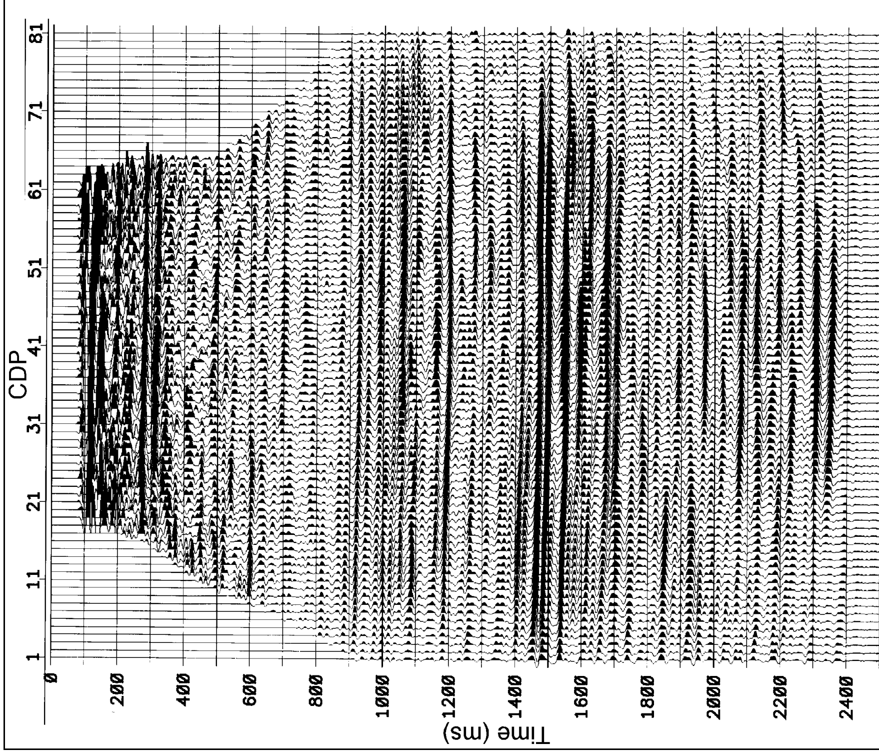

Figure 5. Surface vertical channel stacked section.

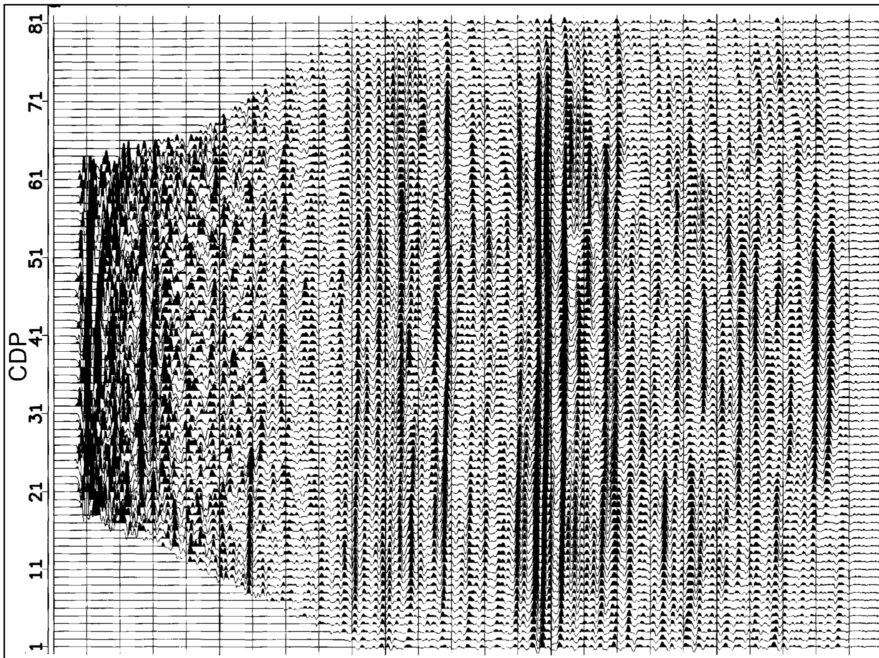

Figure 6. 6m depth vertical channel stacked section.

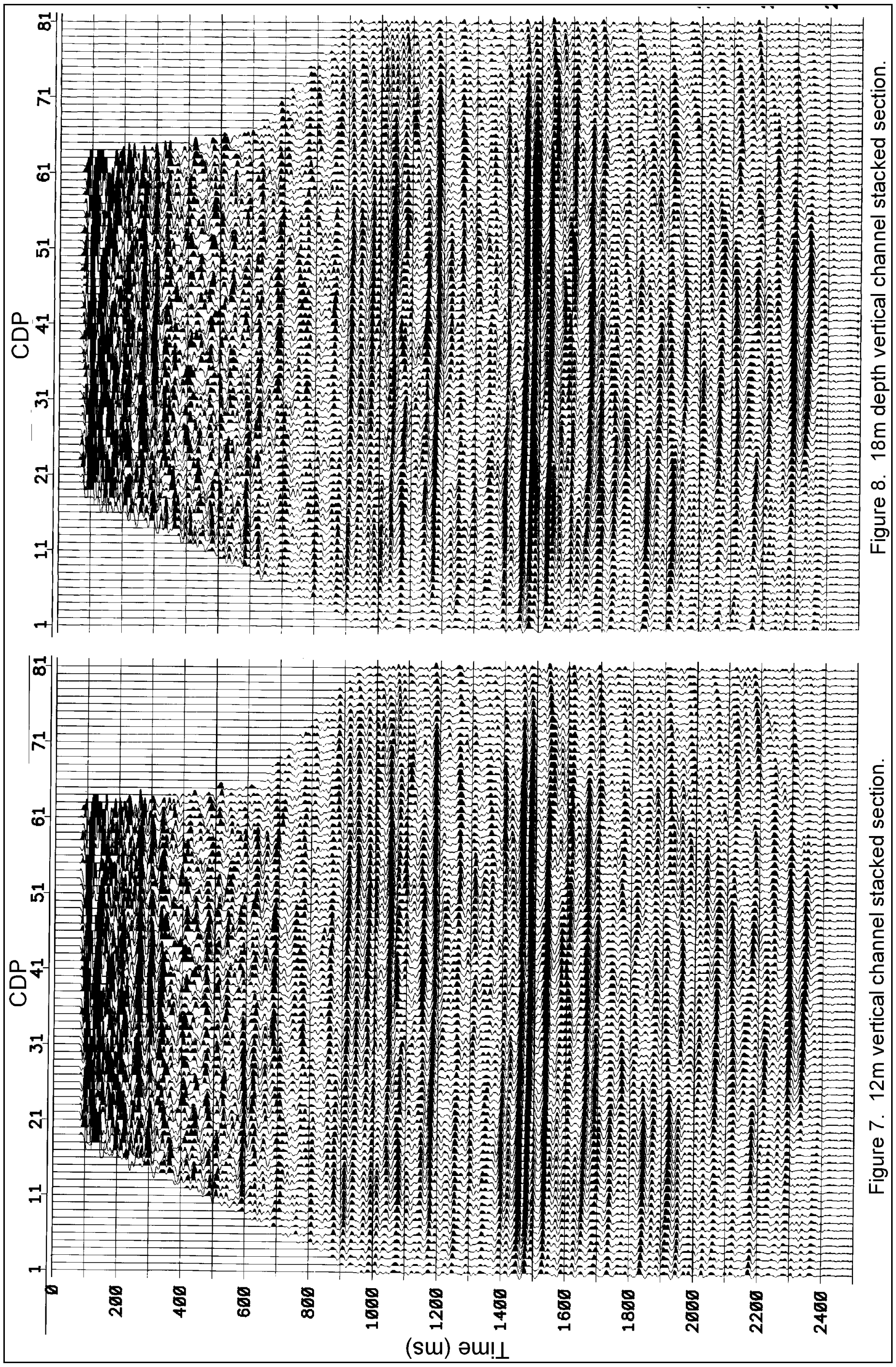

Figure 7. 12m vertical channel stacked section.

Figure 8. 18m depth vertical channel stacked section.

Geometry Assignment

Bin data by ACP

Traces binned assuming Vp/Vs=1.9; bin size=25m

True amplitude recovery

4db/sec gain and correct for geometric spreading

Surface-consistent deconvolution

Polarity correction

Flip polarity of trailing spread

Trace math *or* receiver re-orientation

Sum radial and transverse channels, or *apply horizontal channel re-orientation (buried phones only)*

Time-variant spectral whitening

Balance frequencies between 6 and 80 Hertz

Elevation Statics

Calculated using elevations and uphole shot times

Velocity Analysis

Receiver hand statics

Receiver event alignment

Residual statics

Correlation autostatics

NMO correction

No stretch mute

Top mute

Bottom mute

Time-variant scaling

ACP stack

15% alpha-trim mean

Bandpass filter

6-10-60-70 Hertz zero phase Ormsby

Trace equalization

Migration

Phase shift time migration @ 110% stacking velocities

The radial channel stacked sections for all geophone depths appear in Figures 9-12. The surface data have the highest data quality for reasons discussed in the next sections.

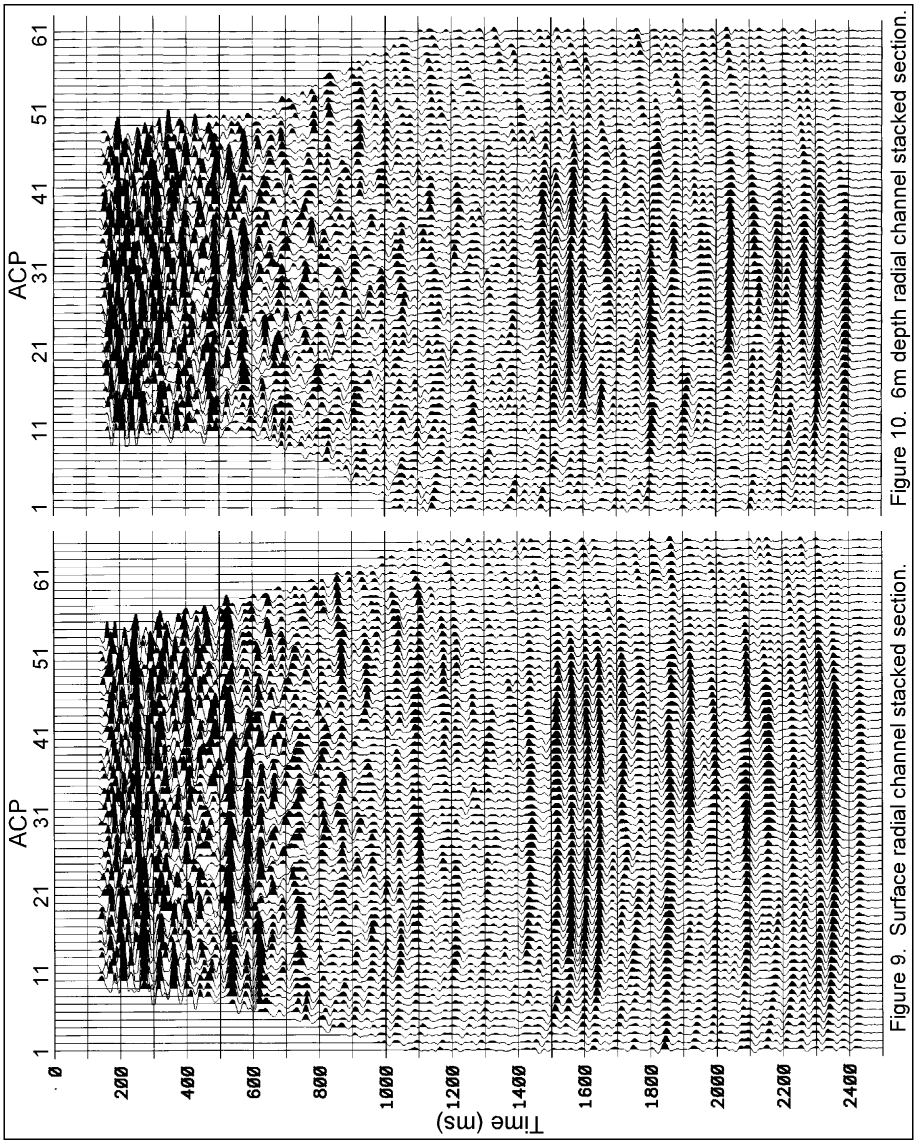

Figure 9. Surface radial channel stacked section.

Figure 10. 6m depth radial channel stacked section.

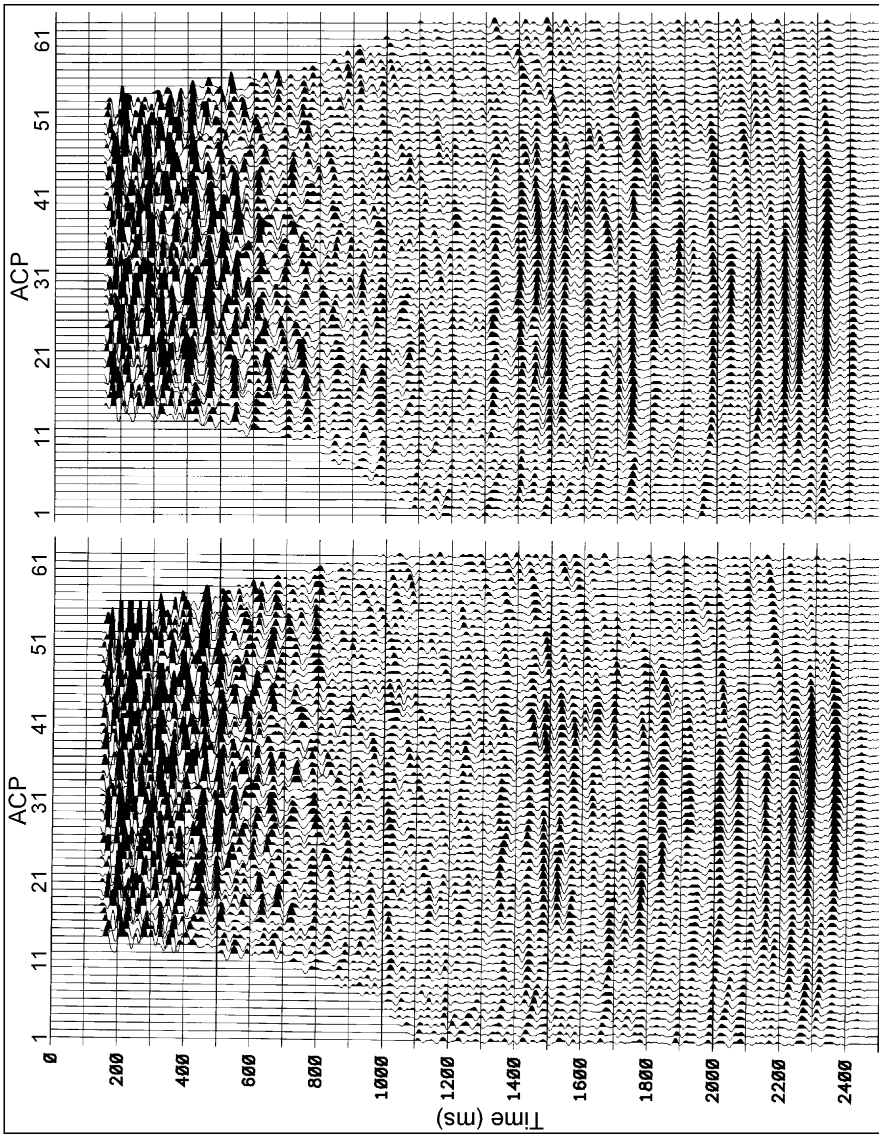

Figure 12. 18m depth radial channel stacked section.

Figure 11. 12m radial channel stacked section.

P-S Asymptotic Binning

The trace binning strategy differs between vertical and radial-channel data, because the source-receiver midpoint does not in general represent the point of mode conversion. Instead, the conversion point asymptotically approaches the point $x_c = x\gamma/(1+\gamma)$ at greater depth, where x is the total source-receiver offset and γ is Vp/Vs (Fromm *et al*., 1985). The variable x_c is referred to as the asymptotic conversion point (ACP), and is about 2/3 closer to the receiver than the source for a Vp/Vs of 2.0. This binning method is a good approximation of the true depth-variant common conversion point. The data for the buried geophones were binned to a 25 meter ACP spacing, assuming a Vp/Vs of 1.9. This value was chosen based on interval Vp/Vs values for an earlier 3D survey acquired in the Blackfoot area (Yang *et al*., 1996).

Mode Leakage and Receiver Re-orientation

Some degree of mode leakage was observed in roughly half of the buried geophone data. The types of mode leakage encountered were compressional-wave reflections on the radial channel and converted-wave reflections on the vertical channel. This is a problem that affects signal-to-noise ratios in converted-wave sections.

Some success at reducing mode leakage was met using receiver re-orientation. Since three-component geophones record particle motion in all three dimensions, the orientation of the x, y and z axes is, strictly speaking, arbitrary, and does not necessarily have to correspond to the vertical, radial and transverse components of the geophone. The data can be transferred to new co-ordinate axes using vector projections (DiSiena *et al*., 1984). The resulting traces represent what would have recorded had the receiver been in the new orientation. This is a crucial step in 3C-3D data processing, as converted-wave amplitude is greatest on a horizontal detector that is parallel (radial) to the source-receiver azimuth (e.g. Simin *et al*., 1996). This is not the case for most shots in a 3C-3D survey, so the horizontal traces are automatically re-oriented.

The true orientation of the buried geophones are unknown, and so is determined indirectly through a three-component first break analysis. This is a Promax tool that works on the premise that the first breaks are compressional wave refractions arriving at near vertical, and rotates the vertical and radial component traces so as to maximize the first break energy on the vertical channel. Compressional-wave reflections that come later presumably have the same sense of particle displacement as the compressional-wave refractions, and also would be maximized on the vertical channel. Shear waves have an orthogonal sense of displacement to the compressional waves, so this rotation would also maximize converted-wave reflections on the horizontal channels. The radial and transverse channels are then rotated until the remaining first break energy is maximized on the radial channel. Any energy that cannot be projected onto either the vertical or radial channel is left on the transverse channel.

Figures 13 and 14 demonstrate the automatic three-component rotation on data from an 18 meter depth geophone. The data have been filtered with a 15-25-110-130 Hertz bandpass filter followed by a 500 millisecond AGC. Figures 13(a), (b) and (c) are the pre-rotated vertical, transverse and radial channel common receiver gathers respectively. The gray lines highlight a P-P reflection on the vertical channel receiver gather. These lines are copied onto the radial and transverse channels, and show that the P-P reflection also appears on these horizontal channels. This is a mode-leaked event. After three-component rotation (Figure 14), converted-wave energy is concentrated on the radial channel.

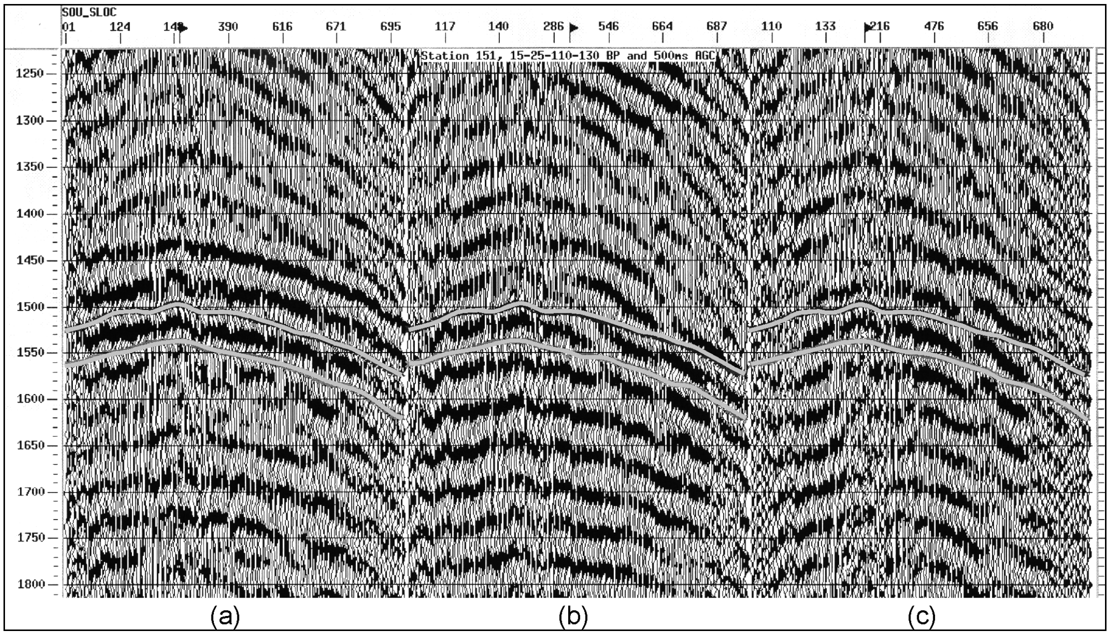

Figure 13. Pre-rotated common receiver gathers for a buried geophone. (a) Vertical channel; (b) transverse channel, (c) radial channel. A P-P reflection, between the gray lines on the vertical channel, also appears on the radial and transverse channels. This is mode leakage.

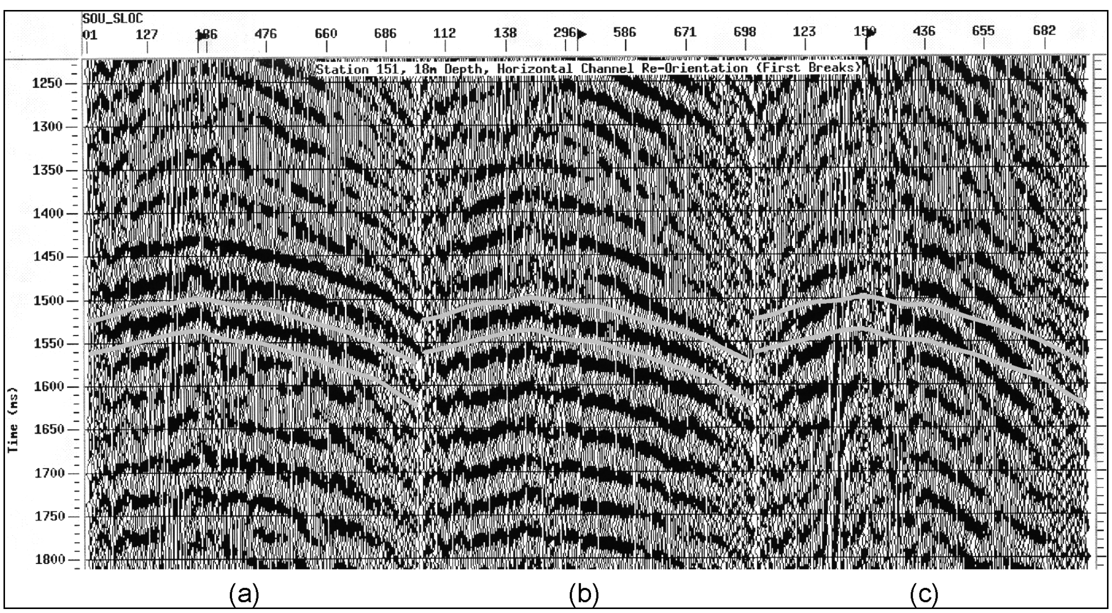

Figure 14. Same as Figure 13 after three-component receiver re-orientation based on first break analysis. Mode leakage has been effectively removed, and converted-wave reflections appears clearly on the radial channel.

This tool reduced mode leakage on only a few buried geophones; normally it was found to have a nominal or even detrimental effect on the data. The tool also tended to reverse the polarity of many traces. The polarity corrections had to be made manually, which was a time-consuming process. Where the automatic re-orientation did succeed, the rotated traces were included in the processing flow.

In cases that converted waves appeared on both radial and transverse channels even after automatic receiver re-orientation was tried, the traces were simply summed to produce a single “horizontal channel” trace for processing. Previous work in the area had not detected any shear wave splitting.

Calculation of Receiver Statics

Receiver statics are of key importance in processing converted-wave data. Typically, the low-velocity layer is much thicker for shear waves than compressional waves as shear wave velocities are relatively unaffected by the water table (Figure 15). Consequently, shear wave statics are almost always larger than compressional wave statics, sometimes by over an order of magnitude (Lawton and Harrison, 1992). This means that, in converted-wave processing, receiver statics are usually larger than shot statics, and the two correlate poorly. Many static correction tools (such as elevation statics) in current commercial seismic data processing software assume that the shot and receiver statics are about the same magnitude and correlate to some degree, and so derive a poor static solution for the converted wave.

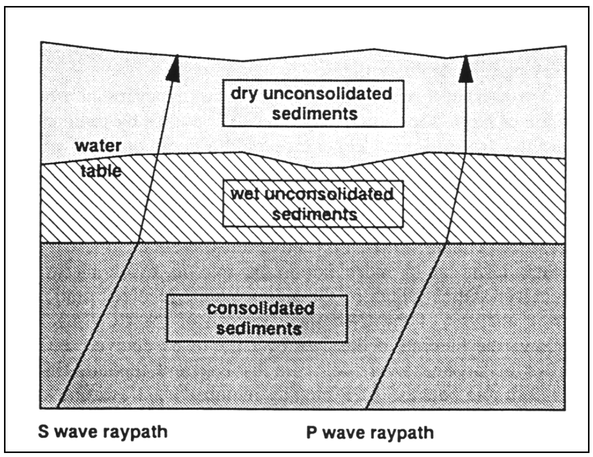

Figure 15. The low-velocity layer is thicker for S-waves than P-waves because S-waves are relatively unaffected by the water table (from Cary and Eaton, 1993).

In order to make conventional static tools effective for converted-wave data, the receiver statics must first be corrected so that they are roughly the same magnitude (or better) as the shot statics. Assuming that the majority of the static for a given trace is receiver static (much greater than the shot, structure and residual NMO statics combined), then an initial receiver static estimation can be made by aligning reflections on common receiver stacks (Cary and Eaton, 1993).

Figure 16(a) is a common receiver stack for the 12 meter radial channel data. Each trace is 144-fold, where NMO-corrected traces from all shots for a given receiver have been summed to create the stacked trace. Reflector continuity is poor (arrow), due to large receiver statics. Continuity improves after a reflection peak is aligned with hand statics (Figure 16(b)). First, a peak (or trough) of the same reflection is picked across all the traces with the horizon picking tool. Then the average time of all the picks is subtracted from each individual pick, and applied to the traces as a static shift. Another iteration may be required for the optimal hand static solution.

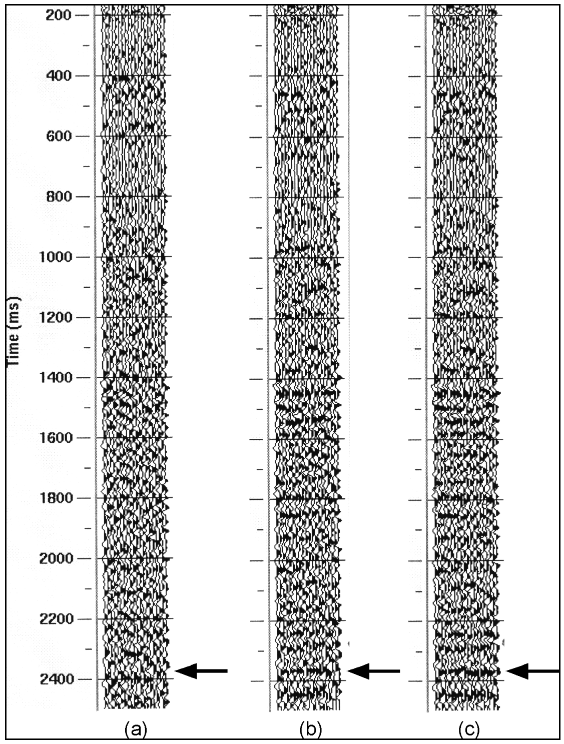

Figure 16. (a) Raw radial channel common receiver stack of the 12 meter depth geophones. (b) Hand statics improves reflector continuity (arrow). (c) Improved overall continuity and resolution of long-period static results after event alignment.

Hand statics are limited in that they tend to best align only the particular reflection that was used for hand statics. Reflections elsewhere may not be aligned optimally, due to noise at the location of the horizon pick. The ideal static would align not just a single reflection at a discrete time, but all the reflections across a large time window. This was done using the event alignment tool. This tool works by first stacking together a user-defined number of traces from the hand-aligned receiver stack to create a model trace. Then it correlates the model trace against each trace in the section over a user-defined time window. The time of maximum correlation of each trace with the model trace is applied as a static. Figure 16(c) shows the receiver stacked traces with event alignment for reflections between 1300 and 2300 ms. In this time window, reflected events exhibit improved continuity compared to hand statics alone (Figure 16(b)) A long-period static has also been removed.

At this point, receiver statics have been resolved sufficiently to produce a brute stack, after which residual statics may be calculated.

FREQUENCY ANALYSIS

If the near-surface is attenuating the signal measurably, it is possible that this attenuation varies along the receiver line. Margrave (1998), for example, found P-P signal bandwidth changed along the profile of a nearby 2-D survey. It is also possible that the shallower geophones will have a more attenuated signal, particularly the converted wave, for reasons mentioned in the introduction.

Prior to frequency analysis, the signal was enhanced by passing the data through an f-k filter that suppressed ground roll, refractions and incoherent noise in the data. Pad (i.e. zero-value) traces were first inserted into the receiver gathered data to keep trace spacing at an even 20m, as there were some skipped and skidded shots in the survey, and f-k filtering works best when spatial sampling is constant or nearly so. For the vertical data, the operator had dimensions 500ms $\times$ 50 traces, with a value of 95% used for time ramp flattening and offset ramp flattening, and a 90% flattening prior to f-k filter windowing. The radial data filter parameters were identical, except that operator dimensions were 750ms $\times$ 100 traces.

Compressional-wave reflections between 1 and 2 seconds were found to be strong for the f-k filtered data, except at very near offsets. For the vertical channel frequency analysis, therefore, the full range of offsets were used. P-S reflection amplitudes were only strong for mid- to far-offsets owing to weak mode conversion at near offsets, so only offsets greater than 600 meters are used in the P-S frequency analysis.

As previously mentioned, signal bandwidth may depend on both receiver location (i.e. its location along the receiver line) *and* receiver depth. The relationship between frequency content, receiver location and receiver depth can be depicted clearly by plotting the spectra data in three dimensions with contour plotting. For every receiver gather of a given depth, a Matlab computer function calculates a separate frequency spectrum in the appropriate time window. It then inserts the frequency spectra columnwise into a matrix in receiver station order. The columns of the resulting matrix represent location along the receiver line; the rows represent frequencies from zero to nyquist; and each individual cell contains decibels below maximum amplitude of the frequency spectra. The program then displays the matrix as a grayscale contour plot with the appropriate colour bar and axes labels.

Vertical Channel

Figures 17 (a) through (d) are frequency contour plots of the vertical channel of the 18m, 12m, 6m and surface geophones respectively. The vertical white bars on some of the plots indicate data gaps due to receiver kills.

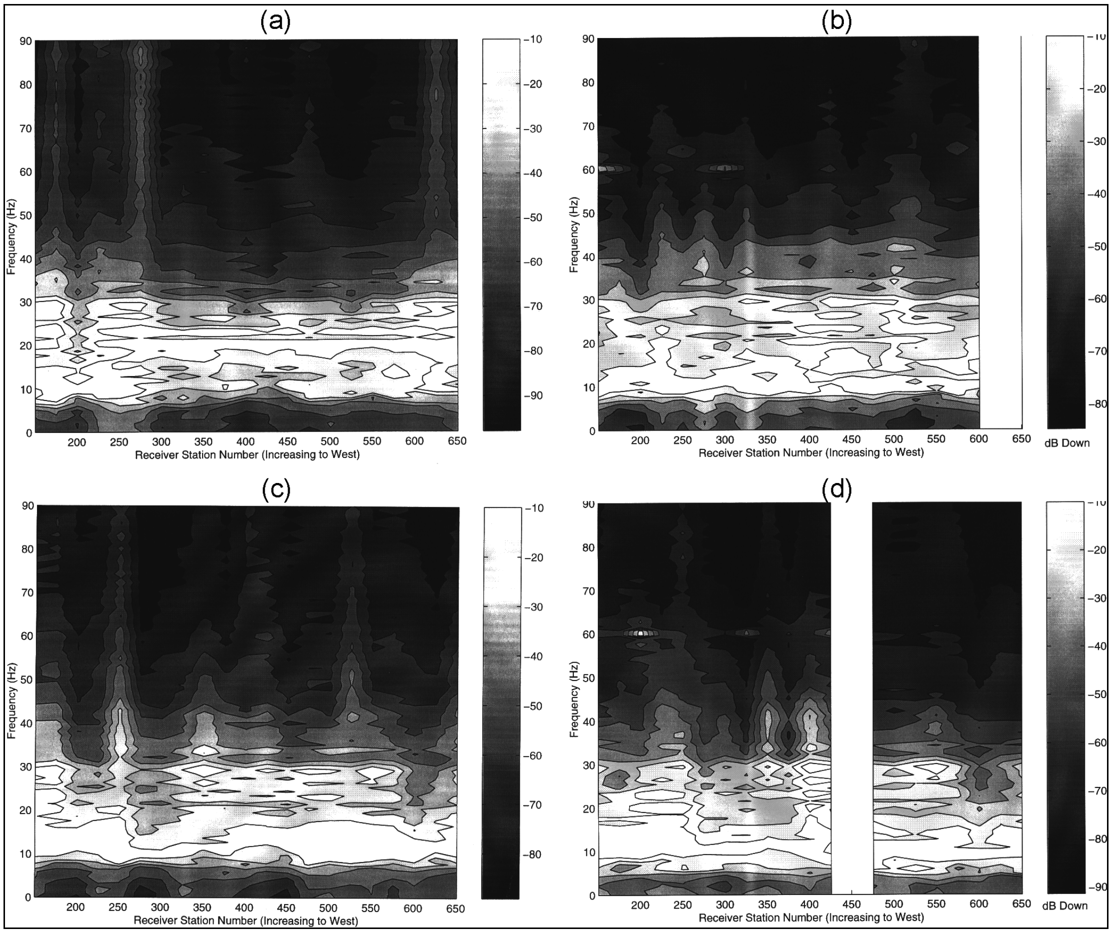

Figure 17. Frequency analysis of the vertical channel (a) surface, (b) 6 meter, (c) 12 meter and (d) 18 meter depth geophones. White vertical bars represent data gaps due to receiver kills.

Between the receivers of any given depth, there exists significant variations in signal bandwidth. For example, in receiver station 326 in Figure 17, the amplitude of the signal falls to about 50 decibels below maximum at about 35 Hertz. The signal of the adjacent receiver gather, station 351, does not decline to 50 decibels below maximum until about 55 Hertz. Reflection bandwidth decreases again for station 376 to values similar to station 326. Note that this frequency variation occurs over only 100 meters of the receiver line. This pattern of adjacent geophones having significantly different signal bandwidths occurs for all depths, and is responsible for the re-entrant contours seen best at frequencies above 40 Hertz.

Between geophones of different depths the frequency spectra correlate poorly. There is no general pattern in the frequency profile that holds for all depths. This indicates that the signal bandwidth patterns in the plots are not station consistent, and therefore probably not due to the effect of increasing overburden thickness attenuating the signal.

The likely controlling factor in these data is geophone coupling. As mentioned previously, the surface geophones were planted by hand and the buried geophones were planted with wooden poles. Planting by hand enabled more consistent ground-geophone coupling than can be achieved with planting by pole, because better pressure control is possible when hand-planting. This is probably why the hand-planted surface geophones show relatively less variation in bandwidth than do the buried phones.

The frequency of the recorded signal of the surface phones differs from the buried phones also. The maximum amplitudes (inside the white contours) occur between 17 and 30 Hertz for the surface phones across most of the receiver line. The signal recorded by the buried phones has peak amplitudes confined mostly between 10 and 20 Hertz. This is the opposite of what would be expected if the overburden was attenuating signal measurably; again this suggests that the controlling factor of signal bandwidth is quality of geophone plant.

One last indication that receiver coupling is the dominant factor in recorded signal bandwidth is the 60 Hertz contamination that can be seen in the 18m and 6m plots (Figures 17(b) and (d)). This noise may originate from buried electrical wires and electrically powered machinery at the nearby 09-08 well, and should be fairly consistent between different geophone depths of the same receiver station. However, the 60 Hertz noise does not correlate between the 18m and 6m contour plots, and is nearly absent in the 12m and surface contour plots.

Radial Channel

Figures 18 (a) through (d) show contoured plots of the frequency spectra of converted-wave reflections for all geophone depths as recorded on the radial channel. At all depths, the P-S reflections have a dominant bandwidth between 8 and 30 Hertz, and there is very little converted-wave data at higher frequencies. Maximum amplitudes (inside the white contours) occur between 10 and 15 Hertz. This is a much narrower bandwidth than the P-P reflections, as expected.

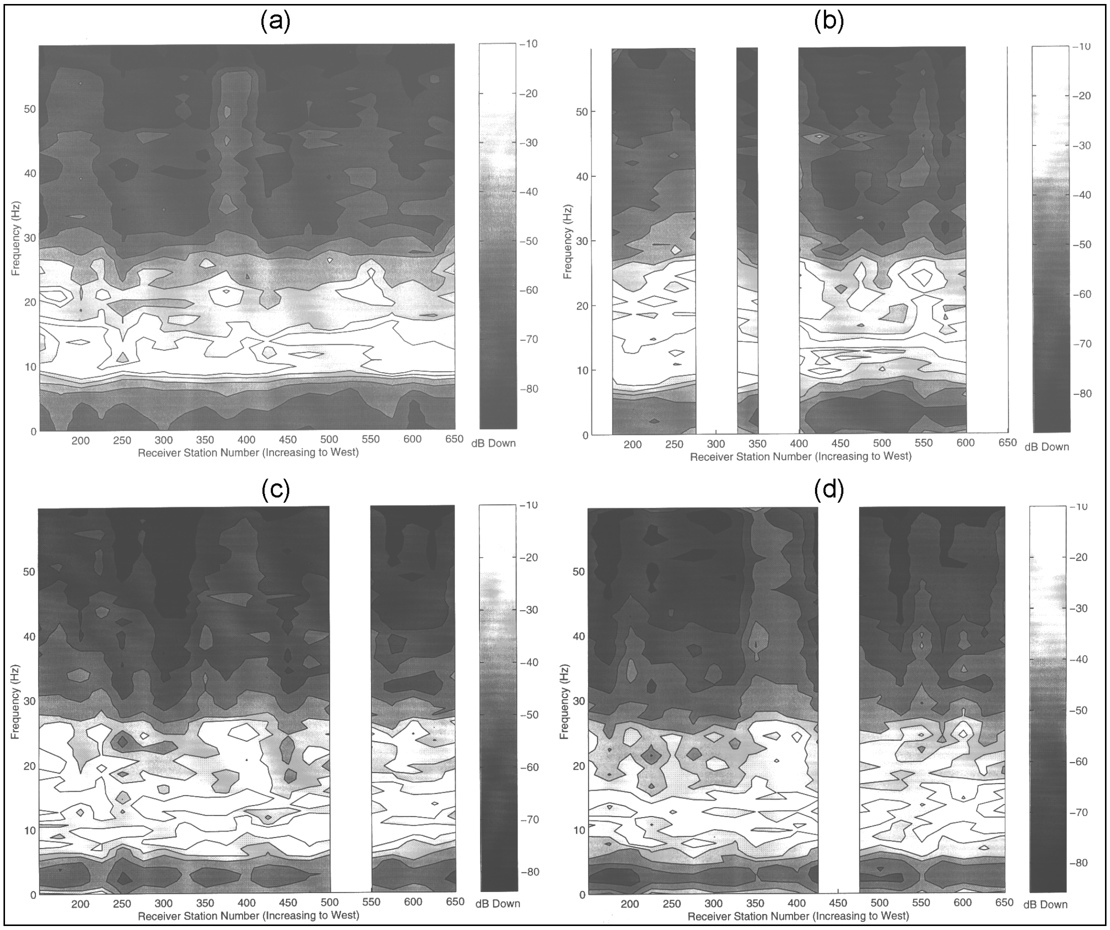

Figure 18. Frequency analysis of the radial channel (a) surface, (b) 6 meter, (c) 12 meter and (d) 18 meter depth geophones. White vertical bars represent data gaps due to receiver kills.

As was found for the vertical channel, there exist considerable differences in bandwidth within geophones of a single depth, yet these differences correlate poorly between the different depths. The surface geophones do not have as great a variation in bandwidth across the receiver line as the buried phones. Again, these observations are considered to indicate variations in geophone coupling.

There appears to be no systematic improvement of converted-wave bandwidth with depth. Any improvement in converted-wave bandwidth that might be gained by burying the geophones is dominated by the effect of geophone coupling.

VERTICAL INTERVAL VELOCITIES

Interval compressional- and shear-wave velocities were determined by the reflection cross-correlation method (Cieslewicz and Lawton, 1997). The P- or S-wave travel time between any two buried geophones of a given station corresponds to the average time of the cross-correlation peak values for windows containing strong, clear reflections. Any geophone interval with a vertical separation of less than two meters has been excluded from this analysis, because events arrive too close in time to provide a reliable determination of velocity.

P-Wave

The time lags determined through trace cross-correlation produced a large range of vertical velocities for approximately two-thirds of the intervals between buried geophones. In certain buried groups, the P-P reflection appears to arrive at shallower depths slightly sooner than at greater depths, resulting in negative apparent velocities (the fact that some 18m geophones were actually shallower than the 12m geophones has been accounted for in these calculations). This experiment may be approaching the limits of accuracy of the geophones and recording equipment. The recording system has a time accuracy of ±1 ms for each geophone. Given this accuracy limit, it is possible that two geophones will record a simultaneous event as having occurred as much as 2 ms apart. For two geophones spaced 5 meters apart in a medium with a P-wave velocity of 3500 m/s, the P-wave travel time between them should be about 1.4 ms. However, a P-wave event travelling between them may be recorded as having arrived at the first geophone 0.6 ms *after* it is recorded by the second, giving an apparent interval velocity of -8300 m/s. The geophones may be affected by a “local static”, which is a time delay caused by low-velocity mud surrounding certain geophones but not others.

P-wave interval velocities between buried and surface geophones yield more consistent and reasonable results (Figure 19). For the western two-thirds of the receiver line, the P-wave velocity for the top 18m of overburden is about 900 m/s. Then there is a sharp increase in P-wave velocity between stations 301 and 226 to values more typical of consolidated sedimentary rock. This likely indicates a thinning of the overburden layer in this area. Velocities peak to an unphysically large value for station 201, and decline somewhat east of this station to values more typical of weathered bedrock.

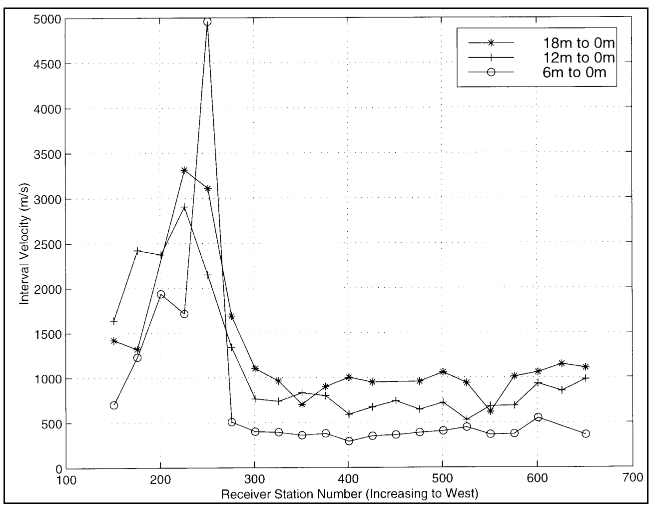

Figure 19. P-wave interval velocities between buried and surface geophones.

The surface to 12m interval velocities show the same general trend as the surface to 18m interval, but this interval has a lower velocity on average. The western two-thirds of the receiver line has a fairly consistent interval velocity of about 700 m/s, followed by an increase to nearly 3000 m/s within the eastern third. Past this point, velocities taper to about 1600 m/s. Again, this indicates that the eastern third of the line has a thinner overburden layer than the western two-thirds.

Velocities between the surface and 6m depth again follow a similar trend, averaging about 400m/s for the western two-thirds and peaking to just under 2000 m/s within the eastern third of the receiver line. The anomalous value of 5000m/s for one station is probably not meaningful.

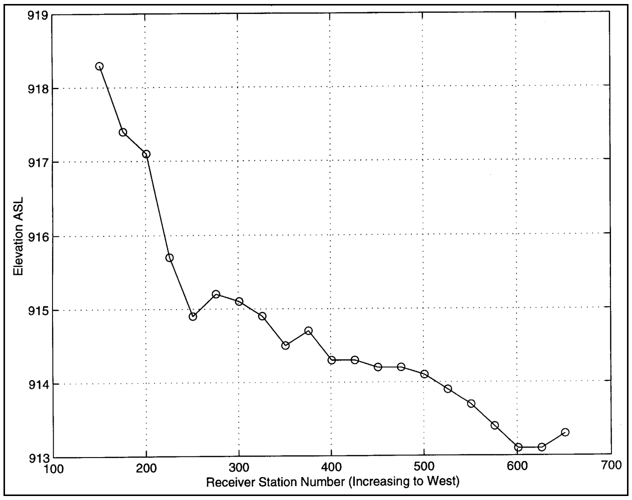

Figure 20. Receiver elevations above sea level (m).

These observations have some consistency with receiver elevation (Figure 20). There is a fairly steady elevation rise of about 0.2 meters per station across the westernmost two-thirds of the receiver line, followed by a much sharper elevation rise for the remainder of the line. The interval velocities peak at the point where receiver elevations change the most. This is demonstrated more clearly in Figure 21, which shows receiver elevation differences between stations from west to east. The point of greatest change in elevation correlates well with the points of greatest interval velocities. This implies that the overburden layer is thinnest at the elevation inflection point, and somewhat thicker on either side of this. Figure 22 shows a schematic velocity model of the near surface that is consistent with these observations.

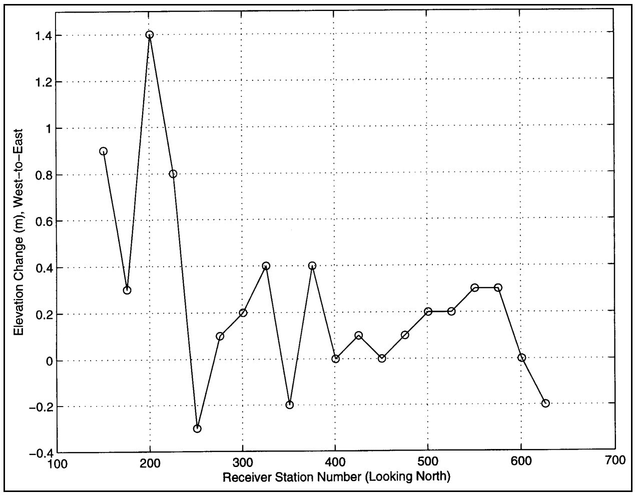

Figure 21. Elevation difference between adjacent geophone stations.

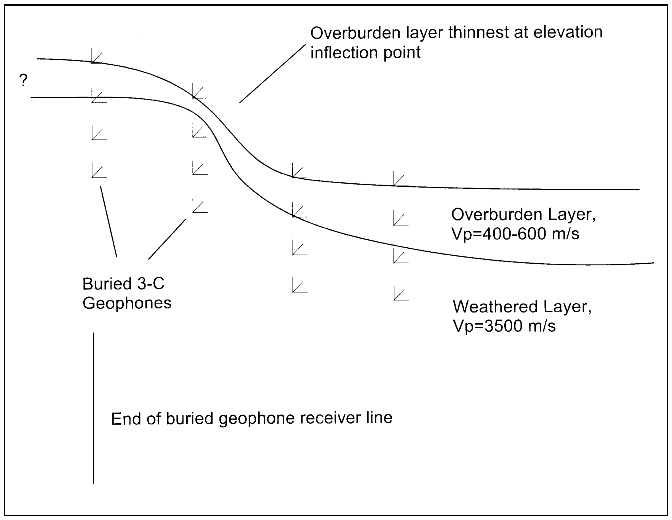

Figure 22. Near-surface velocity model based on P-wave uphole interval velocities.

S-Wave

As previously mentioned, converted-wave reflections recorded by the buried geophones suffered from very low signal-to-noise ratios. This initially resulted in poor correlation values and inconsistent time lags for converted waves ascending through the low-velocity layer. Signal-enhancing f-k filters did not improve correlation values for sufficiently confident shear-wave interval lag times.

This problem was resolved by boosting signal-to-noise ratios through trace stacking. Each radial channel receiver gather was corrected for normal moveout with the same P-S velocity function, with no statics applied. The traces were then muted with top and bottom mutes, and then stacked to produce a single stacked trace for each radial receiver. The stacked traces had a maximum fold of 142, which would (optimally) reduce incoherent noise by a factor of nearly 12. An additional advantage to stacking is that it tends to reduce P-wave energy that has leaked onto the radial channels. This is due to the trailing-spread polarity reversal that has been applied to the traces, which causes converted waves to reinforce during stacking and P-P waves to cancel.

Interval time lags were calculated by cross-correlating the stacked traces of different geophone depths across a time window of 1300 to 2500 ms. This time window contains the zone of interest as well as many other strong converted-wave reflections. The resulting peak correlation values are generally much higher with the stacked traces versus the individual traces of the contributing receiver gathers, and more confident S-wave interval times result.

Figure 23 shows the shear wave interval velocities between buried phones. The 12m to 6m shear wave velocities are average 185 m/s in the western two-thirds of the line, and decrease to an average of 150 m/s for the remainder of the line. The deeper 18m to 12m interval has velocities that are over 150 m/s higher on average than the 12m to 6m interval, but these velocities are far more variable. This may indicate a complex surface of the weathering layer at these depths. The 18m to 6m interval, which encompasses the previous two intervals, shows the same general decrease in velocities toward the east as the 12m to 6m interval, but with highly variable velocities as seen in the 18m to 12m interval. Ideally, the 18m to 6m interval velocity should fall about midway between the 18m to 12m and 12m to 6m interval velocities, but this would only be true if the 12m phone was located exactly midway between the 18m and 6m phone, which was rarely the case (Figure 3).

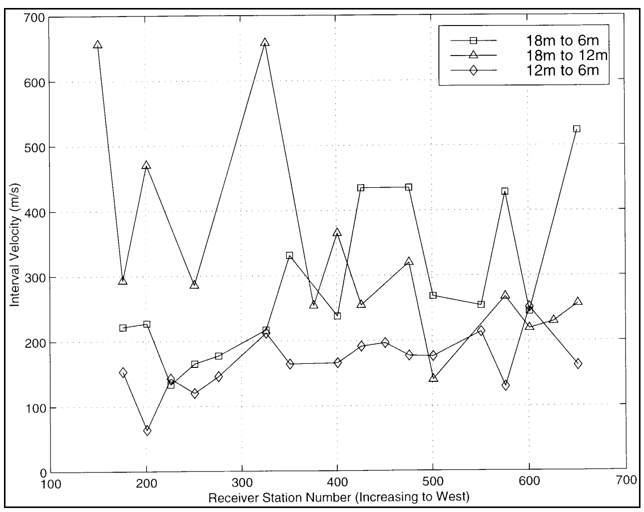

Figure 23. Near-surface shear wave velocities for buried-to-buried intervals.

Figure 24 shows interval velocities between surface and buried phones. The surface to 18m depth has an average shear-wave velocity of 193 m/s. There is a peak in velocities between stations 501 and 476, and a drop between stations 301 and 176. The surface to 12m interval has an average velocity of about 148 m/s, with a general west-to-east decline in velocities until station 201. East of this station, velocities increase rapidly to almost 200 m/s. The surface to 6m interval has shear wave velocities that correlate very well to the surface to 12m interval, and are on average about 20 m/s lower.

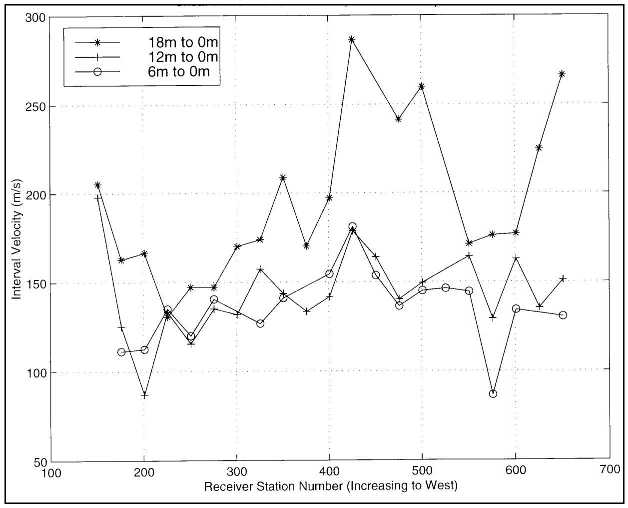

Figure 24. Near-surface shear wave velocities for surface-to-buried intervals.

Most of the profiles show a general decrease in shear-wave velocities from west to east across the receiver line, where a minimum is reached somewhere between stations 201 and 301. East of this area, velocities increase somewhat. The velocity profile has a crude negative correlation with elevation for the western two-thirds of the receiver line. It is possible that strata at the overburden/weathering layer contact have been truncated by erosion, thereby exposing slightly different lithologies at the bottom of the overburden layer across the 1000-meter long receiver line. If the different lithologies have different shear-wave velocities (either inherently or due to differential weathering), this would explain why shear-wave vertical interval velocities change along the receiver line.

Vp/Vs Analysis

As expected, the compressional- and shear-wave velocity profiles of the near surface do not correlate well. While P-wave velocities peak dramatically between stations 151 and 301, S-wave velocities actually decline slightly in this interval.

The resulting Vp/Vs plots for surface-to-buried geophones (Figure 25) show that the Vp/Vs is fairly constant between stations 151 and 301. The top 6m has an average Vp/Vs of 2.8 in this region, the top 12m has an average Vp/Vs of 5.1 and the top 18m of the low-velocity layer has a Vp/Vs of 4.7. East of station 301, Vp/Vs values become unphysically large; values over 20 have been excluded from the plot. The large Vp/Vs values between stations 301 and 176 occur due to high P-wave velocities (Figure 19), and not due to a drop in S-wave velocities.

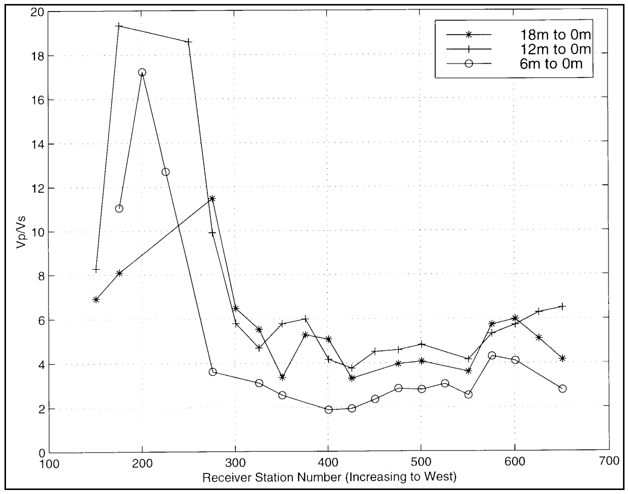

Figure 25. Vertical interval Vp/Vs values for surface to buried geophones.

Vp/Vs values between buried geophones do not produce meaningful results, as a result of the extreme (and sometimes negative) interval P-wave velocities.

SIMILARITY OF STACKED SECTIONS

Although the stacked sections in Figures 5-12 are visually similar, their similarity can be determined using trace differences, cross-correlations, and mean square difference. The receivers of a given buried geophone station are only a few meters apart, and so record essentially the same wavefield. Since data from the four geophone depths were acquired simultaneously and processed the same, their similarity should be controlled by the effects of burial on recorded signal and random noise.

Trace Differences

A simple and direct way to determine the similarity of two seismic sections is to take their difference; this is the usual procedure in time-lapse seismic studies. Before sections can be subtracted from each other, their reflected data must be aligned as precisely as possible. The completely processed sections had residual static differences of up to 20 milliseconds (see lag times in Figures 28 and 29), because reflections arrived at deeper geophones first (see previous section), and these timing differences carried through to the final stack. Trace pairs (i.e. the same CDP trace from two different sections) to be subtracted were first cross-correlated across a portion containing strong reflections. The time lag of the peak value of the resulting correlogram was then applied as a trim static to one of the traces, which aligned the reflections precisely. Then their difference was taken. The procedure was repeated for all traces in the sections to be compared, resulting in a “difference section”.

Figure 26 shows the vertical channel data from the 12 meter stacked section, the 6 meter stacked section, and their difference as determined by the above method. Trim statics have been applied to align reflections in the two sections. There is strong signal in the stacked sections, but almost nothing in the difference section, indicating that the reflected data is virtually the same. The linear noise in the difference section may be the branches of off-line diffractions caused by irregularities at the top of the bedrock (the apices of the diffraction hyperbolae do not stack constructively (Larner *et al*., 1983)). They are present in both input sections, but become more noticeable with the high-amplitude reflections are removed. Similar results were found for other stack differences, indicating a high degree of experimental repeatability for the buried geophone experiment.

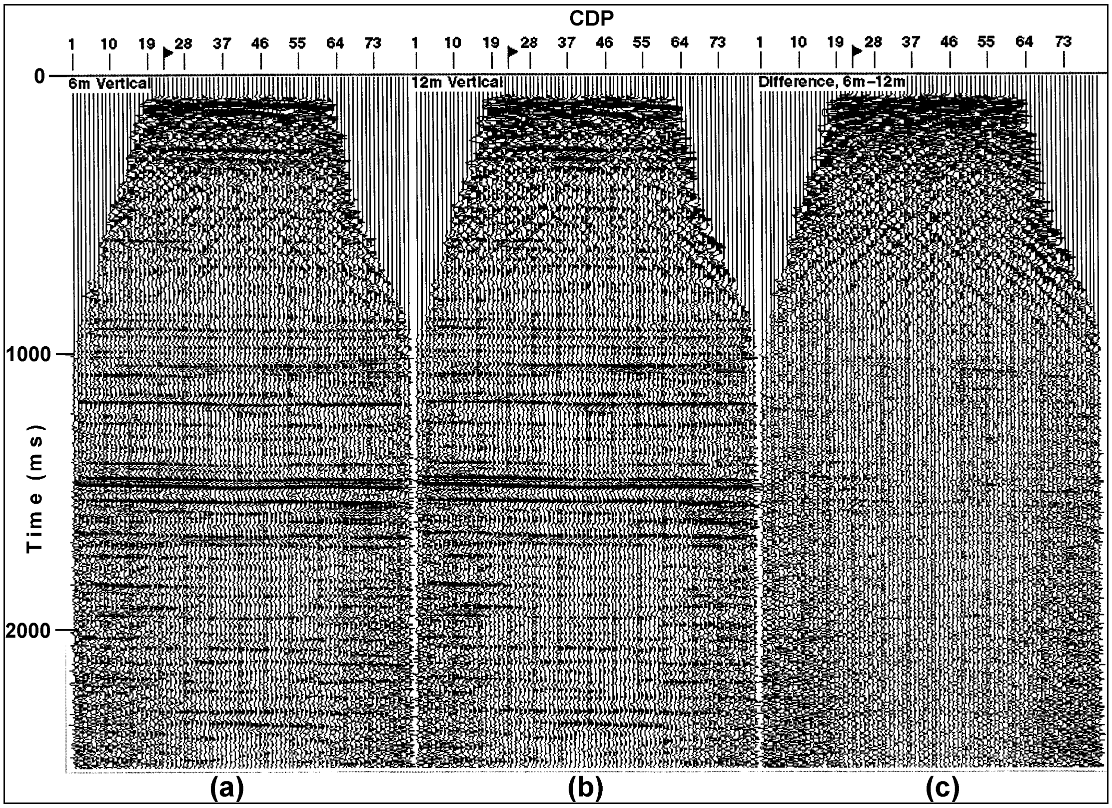

Figure 26. The (a) 6 and (b) 12 meter vertical channel stacked sections, and (c) their difference, which is mostly random noise.

The identical procedure was applied to the radial channel data. Figure 27 shows an example of the surface and 12 meter radial channel stacked sections, and their difference. The trace subtraction removes most of the signal, leaving essentially random noise in the difference section. This was found for other radial channel difference sections as well. The linear noise at early times did not emerge on the difference sections of the radial channel data, indicating that the diffracted energy was composed chiefly of compressional waves, as it did not stack constructively with P-S velocities and ACP binning. In general, this experiment indicated a high degree of experimental repeatability for converted-wave data as well.

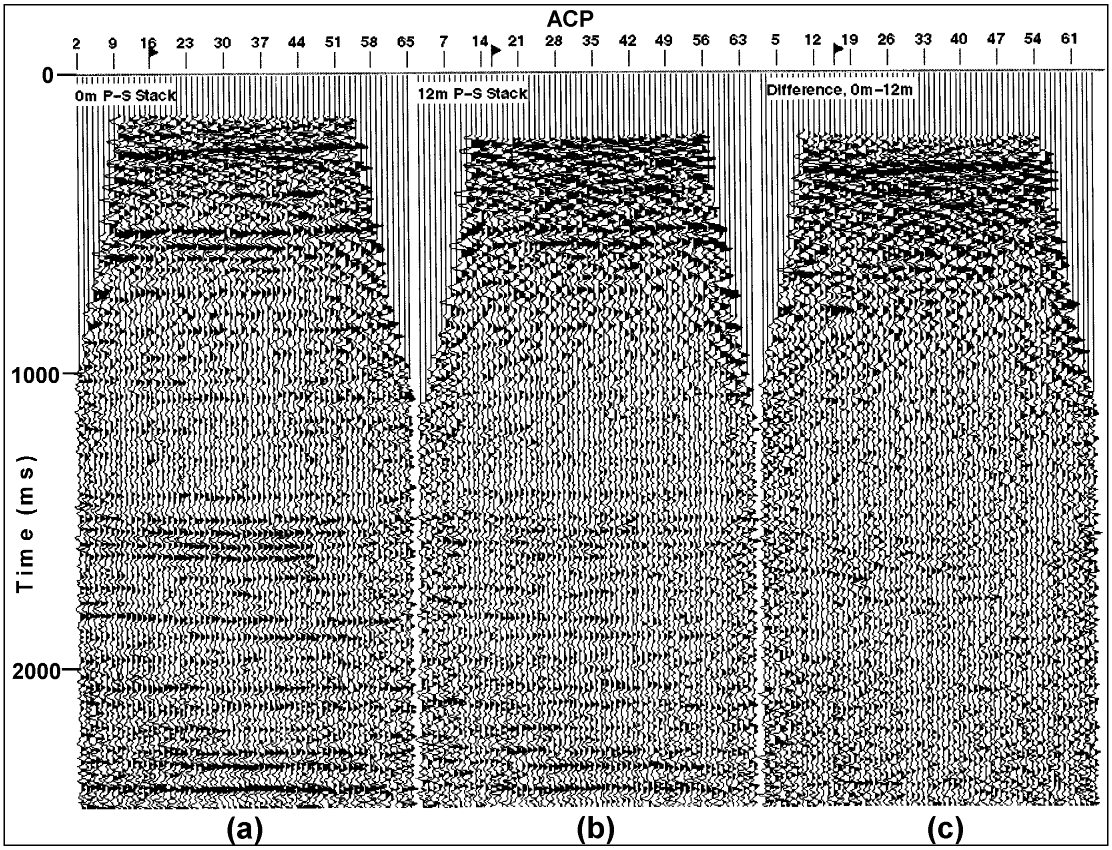

Figure 27. The (a) 0 and (b) 12 meter radial channel stacked sections, and (c) their difference.

Cross-Correlations

Cross-correlation values and lag times were calculated with the same Matlab computer function that was used to obtain interval lag times (see previous section). Both stacked and migrated sections were analyzed as it has been previously demonstrated that migration can improve repeatability (i.e. correlation) in time-lapse seismic studies (Porter-Hirsche and Hirsche, 1998).

Vertical Channel

Cross-correlation values for the vertical channel data were calculated in the 900-2000 ms time window, as this region contained the zone of interest plus numerous other strong, clear reflections. Results using other time windows of different sizes were virtually the same, so this window can be viewed as representative of most of the section.

Figure 28 shows peak correlation values and corresponding lag times between all depths of the vertical channel stacked and migrated sections. To reduce cluttering, results from the six comparisons are displayed on two separate plots. Overall, the stacked sections (Figures 28 (a) and (b)) correlate to each other well, achieving coefficients of over 0.9 in places, indicating that the stacks are very similar to each other. Correlation values are much the same for all comparisons, indicating that no two sections are particularly similar or dissimilar. Maximum cross-correlation values are highest at the central, high fold portions of the stacks, taper off slowly towards the edges of the section, and drop off sharply at the very edges. This pattern correlates to fold (Figure 4(a)), which decreases from the center of the stacked sections. The very pronounced decrease in correlation at the edges occurs where the fold drops to below about 12. Since signal-to-noise ratio is proportional to fold, much of the observed correlation patterns in Figure 28 can be attributed to non-correlatable random noise in the data.

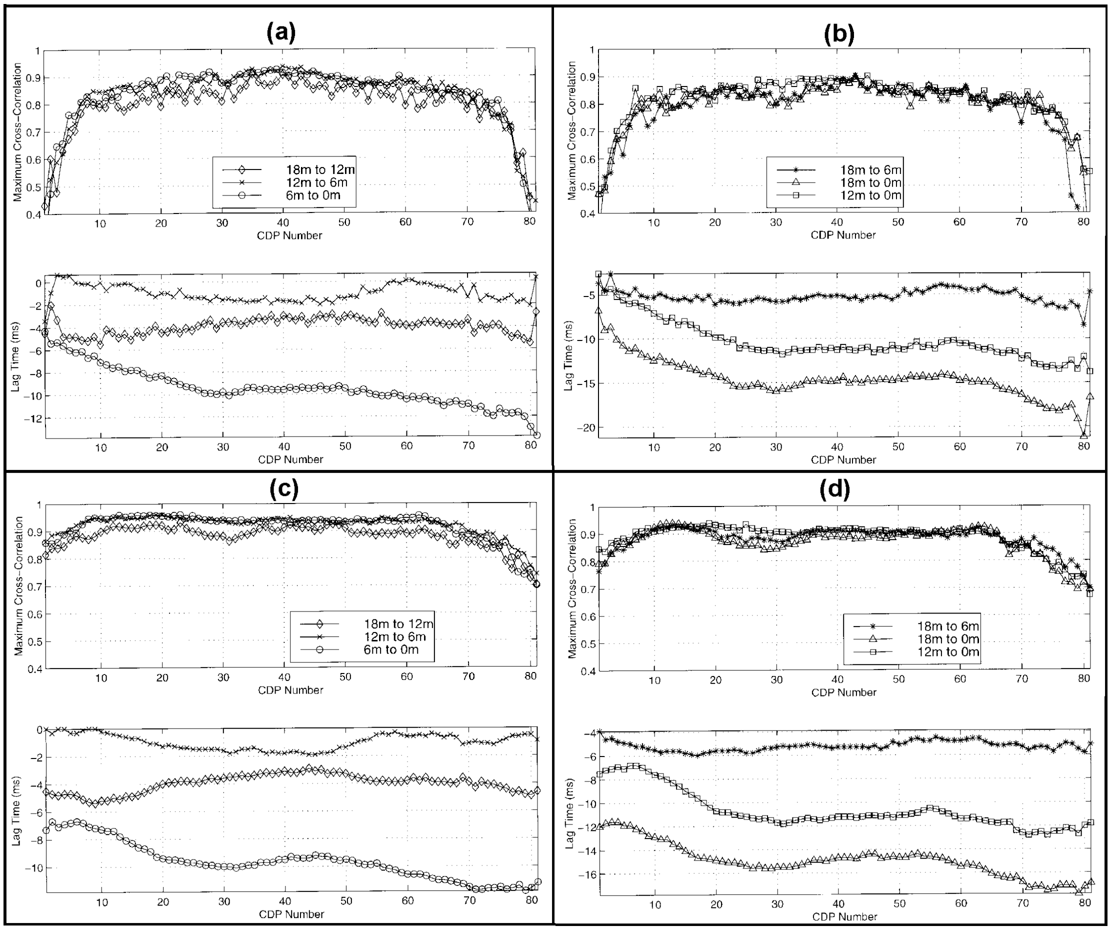

Figure 28. Vertical channel section correlation analysis for the (a) and (b), stacked sections; and (c) and (d), migrated sections.

As anticipated, the migrated sections (Figures 28 (c) and (d)) have higher maximum cross-correlation coefficients than the stacked sections, both on average (Table 1) and by peak value. Correlation values are fairly flat through the central four-fifths of the migrated sections; the stacked sections for the same region show a gradual decrease toward the edges. At the very edges, correlation values taper moderately to a minimum of about 0.7, which is much larger than the comparable value for the stacked sections. The results clearly demonstrate the noise-suppressing effects of migration, which is particularly acute for low fold regions of a section. Migration not only improves signal-to-noise ratios, but balances it better throughout

Contents

the whole section. Table 1 shows that while migration improves absolute similarity between sections, it does not change their relative similarity.

	Average Cross-Correlation			
Group Interval (m)	**Stacked**	**Rank**	**Migrated**	**Rank**
18-12	0.8445	4	0.9005	4
18-6	0.8423	5	0.8985	5
18-0	0.8367	6	0.8866	6
12-6	0.8851	2	0.9388	2
12-0	0.8600	3	0.9114	3
6-0	0.8883	1	0.9419	1

Table 1. Average peak cross-correlation values of the vertical channel stacked and migrated sections for CDPs 15 to 65. Time window is 0.9 to 2.0 seconds.

Table 1 reveals several patterns in section similarity. A relation exists between spatial closeness of two section and their similarity; groups separated by 6 meters have greater similarity than groups separated by 12 meters, which in turn are more similar than groups separated by 18 meters. There is also a tendency for shallower sections to be more similar to each other than deeper sections. Thus the 6m and 0m sections are more similar than the 6m and 12m sections, which in turn are more similar than the 12m and 18m sections, even though each section is separated by 6 meters.

Random noise levels undoubtedly play a factor in these results. Reflection amplitudes display a clear depth relation to depth, as the near surface acts as a natural signal amplifier (Chapter 3). This would result in better signal-to-noise ratios for shallower geophones, which would tend to increase correlation values. Therefore, the deeper sections correlate more poorly than the shallower sections because they contain more random noise. The tendency of sections that are closer spatially to have higher correlation may be due to the similarity of receiver notches in the frequency spectra (Chapter 3), though this is not evident from the frequency spectra of the raw or stacked data.

Radial Channel

A time window of 1000 to 2200 milliseconds was used to calculate the radial channel cross-correlation values, which contained abundant converted wave reflections. Figure 29 (a)-(d) shows the peak correlation values and time lags for the stacked and migrated sections. Cross-correlation values are much lower for converted wave reflections than compressional wave reflections (previous section), because the smaller reflection amplitudes result in lower signal-to-noise ratios. The stacked sections in Figures 29 (a) and (b) show that correlation values peak in the central, high-fold portion of the section and taper off gradually toward the edges. There is no sudden drop-off as there was for the vertical channel data, indicating more overall consistent (but higher) random noise levels across the sections. The correlation values tend to fluctuate within this general trend though, indicating a lower degree of similarity in these sections. The fluctuations become more pronounced after migration (Figures 29 (c) and (d)). While some correlation values increase after migration, others have become lower. Migration decreased average correlation values in half the section comparisons (Table 2). This may be due to migration artifacts that correlating poorly between sections, as a result of poor signal to noise ratios originating in the stacked sections.

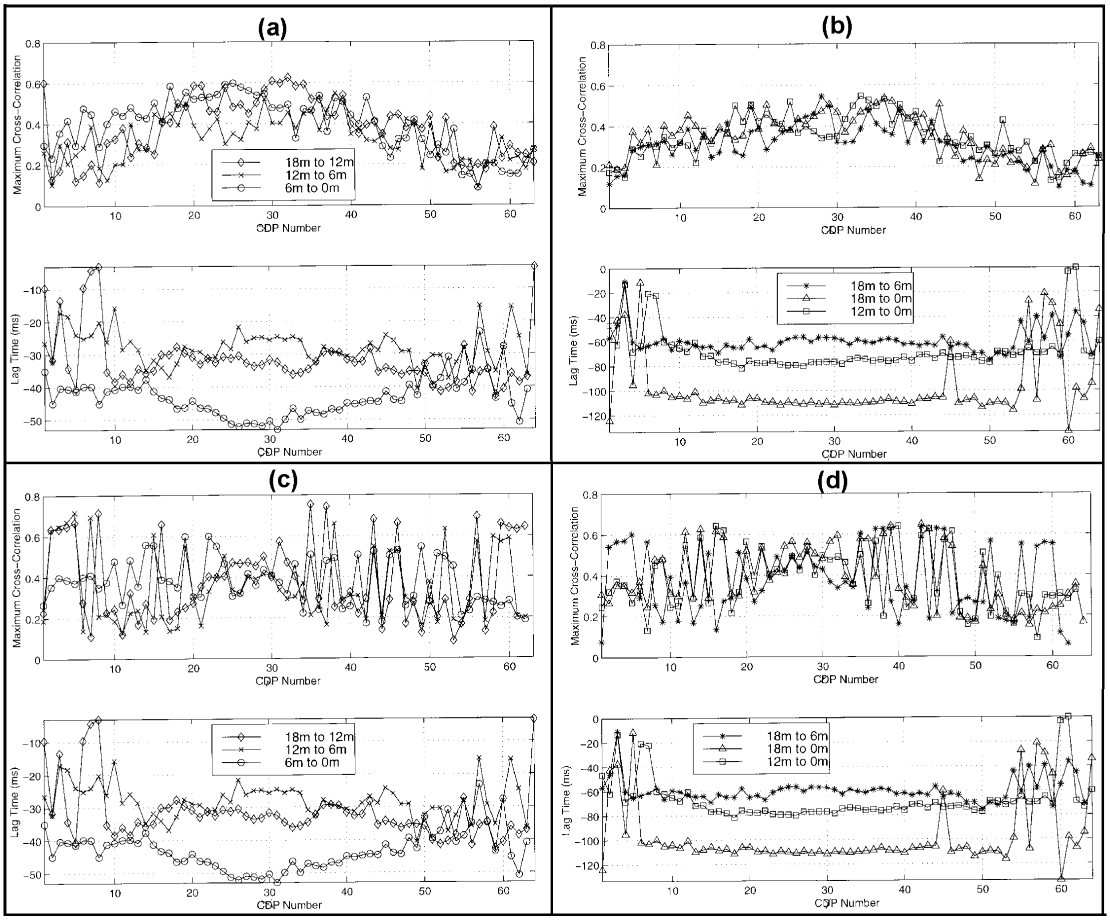

Figure 29. Radial channel section correlation analysis for the (a) and (b) stacked sections; and (c) and (d), migrated sections.

	Average Cross-Correlation			
Group Interval (m)	**Stacked**	**Rank**	**Migrated**	**Rank**
18-12	0.4306	2	0.3439	5
18-6	0.3381	6	0.3630	4
18-0	0.3801	4	0.4255	1
12-6	0.3574	5	0.3169	6
12-0	0.3833	3	0.4116	2
6-0	0.4367	1	0.3956	3

Table 2. Average peak cross-correlation values of the radial channel stacked and migrated sections, for ACPs 10 to 55. Time window is 1.0 to 2.2 seconds.

Results from the radial channel cross-correlation analysis are summarized in Table 2. Some of the same general trends seen in the vertical channel data (Table 1) also appear in the radial channel data. For example, the surface and 6 meter are the most similar of all the sections, as they were for the vertical channel data. Before migration, it can be seen that closer geophone intervals tend to correlate better than intervals that are more widely spaced, and sections from shallower geophones correlate better than sections from deeper ones. After migration these tendencies are not as clear, as both absolute and relative cross-correlation values between sections are not preserved. The amplitude-depth relation for converted-waves is not as strong as it is for compressional waves (Chapter 3), meaning that the near surface does not amplify shear waves as much as it does compressional waves. Signal-to-noise ratios between converted-wave sections therefore do not vary as much as they do between compressional-wave sections. This is why the vertical channel cross-correlation values are related to receiver depth, whereas the relation is not as clear on the radial channel.

Synopsis

The cross-correlation analysis indicates that the similarity between the sections is mostly controlled by random noise levels, because any factor that reduces random noise (fold, migration, shallower receiver depth, reflection type) tends to make sections more similar to each other. This effect is weaker on the radial channel than the vertical channel data. Sections from geophone levels that are closer in depth also tend to be more similar, which is possibly due to similarities in receiver notching.

Mean Square Difference

The mean square difference provides a quantitative measure of trace similarity that, unlike cross-correlations, has physical meaning for seismic traces. The sample values of a trace represent varying voltages as recorded by a geophone, as it responds to varying particle velocities. Because energy is proportional to velocity squared, and power is energy per unit time, seismic trace values squared are termed the power of the trace (Sheriff and Geldart, p.286), as each sample represents a constant time unit. The mean square difference of two traces, then, is the same as the power of their difference.

Vertical channel stacked and migrated sections were compared in a time window of 0.9 to 2.0 seconds; radial sections were compared over a 1.0 to 2.2 second time window. The mean square difference values were averaged between CDPs 15-65 for the vertical channel, and ACPs 15-55 for the radial channel. Results are tabulated in Table 3.

Geophone Interval	**Stacked Vertical MSD**	**Rank**	**Stacked Radial MSD**	**Rank**	**Migrated Vertical MSD**	**Rank**	**Migrated Radial MSD**	**Rank**
18m-12m	0.4182	3	1.4377	4	0.2400	4	0.8182	4
12m-6m	0.3356	1	1.6141	5	0.1539	1	0.9067	6
6m-0m	0.3510	2	1.4056	1	0.1620	2	0.4993	3
12m-0m	0.4431	4	1.4233	3	0.2353	3	0.4418	2
18m-0m	0.5432	6	1.4319	2	0.3079	6	0.4353	1
18m-6m	0.4670	5	1.6342	6	0.2603	5	0.9039	5

Table 3. Stack similarity results using mean square difference (MSD).

The vertical channel results were similar to those found by the cross-correlation analysis. Vertical channel stacked sections that are closer in space have an strong tendency to be more similar; stacks separated by 6 meters are the most similar while the stacks separated by 18 meters, the least. Stacks separated by 12 meters are of intermediate rank. There is also a tendency for shallower stacks to be more similar to each other than deeper stacks, but this is weak. After migration, the MSD for all intervals has decreased significantly, certainly as a result of improved signal-to-noise ratios. Two intervals that had a close MSD before migration have exchanged rank, but essentially the same observations can be made with regards to similarity of depth and similarity of section.

As anticipated, the radial channel sections have a much higher MSD than the vertical channel sections, as a result of poorer signal-to-noise ratios due to weaker amplitudes of the converted wave. Intervals involving the surface radial data have the lowest MSD, particularly after migration. This may be expected, as the surface data had much better data quality, which would result in lower residual noise after trace subtraction. Other tendencies are unclear.

In summary, the mean square difference indicates that the similarity of vertical channel data is controlled primarily by relative geophone depths and secondarily by absolute geophone depth. That is, sections from closer intervals tend to be more similar than sections that are farther away, and data from shallower sections tend to be more similar than the deeper sections. The primary control may be due to receiver notching, which can be expected to be more similar for geophones of similar depth. The secondary control may be due to higher raw reflection amplitudes in shallower geophones, which would cause higher signal-to-noise ratios and hence lower MSD for data from shallower depths.

The surface radial sections are more similar (have a lower MSD) to the buried sections than the buried sections have to themselves. This is likely the result of a superior signal-to-noise ratios in the surface data, as it was unaffected by problems of mode leakage and poor geophone coupling. The surface data also benefited from higher absolute reflection amplitudes. No other tendencies were clear. Random noise levels are therefore the chief factor in governing the similarity or repeatability of the radial channel sections.

INTERPRETATION

Dufour *et al*. (1998) give an overview of the geology of the producing formation and units surrounding it. There were two important considerations made in the design phase of this experiment in order to assist in interpreting the seismic data. The first is that all experiments of the Blackfoot III seismic survey, including the buried geophone portion, were designed so that fold would be maximum at the mid-point of the producing channel-fill sediments. This was, naturally, to ensure that seismic data quality (in terms of signal-to-noise ratio) was highest across the producing zone. Secondly, the line was situated adjacent to the producing oil well 09-08, for which P-wave and S-wave sonics, as well as density logs, were available.

The full sonic and density logs for the 09-08 well are advantageous, because together they can be used to calculate the P-wave and S-wave impedance of the formations. It is not necessary to make approximations of Vs from regional Vp/Vs values or density from a Gardener's relationship, so the resulting synthetic traces generated are expected to be highly accurate.

Interpretation was done on phase-shift migrated data from the surface geophones, which had the highest data quality in terms of signal-to-noise ratio.

Generation of Synthetic Seismograms from Well Log Data

Converting sonic and density well logs to expected surface seismic expressions was accomplished using software that uses full Zoeppritz equations to determine offset- (i.e. angle-) dependent reflectivity for both P-P and P-S reflections (Margrave and Foltinek, 1995). The reflectivity values at each offset are convolved with a user-specified source wavelet to generate a synthetic offset gather. The traces in the offset gather are then stacked to produce a synthetic common reflection point trace that presumably simulates the seismic response of the formations at the location of the well. It should therefore tie to common reflection point seismic sections at the well location.

The software also converts the formation tops from depth to time, and plots them on the synthetic traces. This makes possible the crucial link between the formation tops and their corresponding peak, trough or zero crossing on the seismic data, which makes data interpretation possible.

The synthetic traces were generated using a 50 meter receiver interval to a maximum offset of 800 meters. The near-surface model was calculated automatically by the program, and not specified, to ensure consistency between different synthetic traces. For the P-P synthetic traces, a zero-phase 5-10-70-80 Hertz bandpass source wavelet was used, as this most closely matched the bandwidth and phase of the stacked data. The P-S synthetics were generated with a zero-phase 5-10-35-45 Hertz bandpass wavelet for the same reason. The log integration interval was 2 ms for P-P and 3 ms for P-S reflections, as recommended by Miller *et al*. (1995) for good matching to the data. No spherical spreading, attenuation or transmission losses were included in the modeling as these effects had been corrected for during data processing. The NMO-stretch effect was not included in the synthetic trace generation, as this was found not have a detectable effect on the stacked traces produced by the program.

Log Splicing

The Blackfoot III line tied to the 09-08 well only, which intersected the Glauconite channel, but did not reach the Mississippian. To interpret off-channel data and reflections from the Mississippian and deeper, it was necessary to splice portions of other well logs into the 09-08 log. For example, the 09-17 log is from a gas-producing well that is slightly off-channel and so, when spliced into the 09-08 log, simulates off-channel response. The 14-03 was a deep well that reached the Cambrian, and its log data are used to interpret deep reflections when spliced to the

09-08 data. Shear sonics were unavailable for the 14-03 well, so an assumed Vp/Vs of 1.9 was used below the splice point. This is approximately the average Vp/Vs value between the Wabamun and Cambrian for the Blackfoot region, as indicated by an earlier 3-D survey (Yang *et al.*, 1996). The 08-08 is an on-channel well that intersected the Mississippian that is relatively close to the 09-08 well. Its relevant intervals are spliced into the 09-08 log to assist in locating the Mississippian reflection.

The Coal 3b marker, located in the Mannville group, was common to all wells and was used as the splice point to interpret regional reflections. The top of the Glauconite was the splice point used to interpret the on-channel Mississippian reflection. Table 4 summarizes the log splicing used for the interpretation of the Blackfoot III data, and gives their informal names used in this section.

Log Name	Top Splice	Bottom Splice	Splice Point
Channel	09-08	-	-
Regional	09-08	09-17	Coal3b
Deep Regional	09-08	14-03	Coal3b
Mississippian Reflection	09-08	08-08	Top Glauconite

Table 4. Summary of log splicing used for interpretation of the Blackfoot III line.

Logs of the 09-17, 14-03 and 08-08 wells were resampled from a 0.3048 to a 0.1524 meter depth interval to match the 09-08 log. The resampling was done using a Matlab program that performs smooth data interpolation with a sinc function.

Channel and Shallow Regional Synthetic Ties

Figure 30 shows the “Channel” and “Regional” P-P synthetic traces inserted into the interpreted vertical channel migrated data for the zone of interest. Selected reflections are interpreted; in general there is good agreement between the “Channel” synthetic traces and the seismic data. The Glauconite channel fill zone corresponds to the last trough on the trace, and a portion of the lower frequency, high-amplitude peak above it. The remainder of the peak corresponds to the Coal 2 and Coal 3 markers, and the trough above that corresponds to the Coal 1 marker (interpreted).

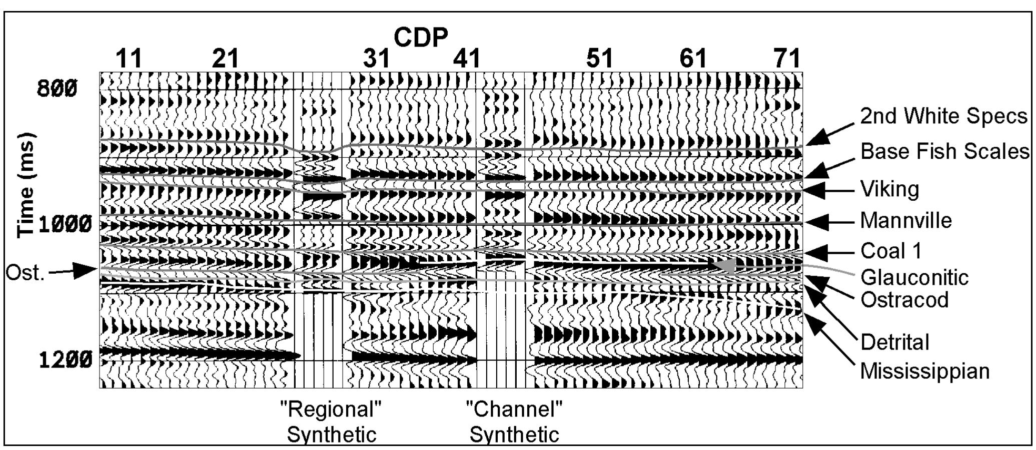

Figure 30. Channel and regional synthetic traces P-P synthetic traces spliced into vertical channel data.

Contents

The regional synthetic traces also show good agreement to the data, with some trace stretching for times earlier than 900 milliseconds. Trace streching is a well known phenomenon caused by short path multiples and frequency dispersion (Stewart *et al*., 1984). This problem can be reduced if the sonic data are check shot corrected, but these data are not. The peak at the bottom of the regional synthetic trace corresponds to the top of the Mississippian, which appears to form a structural low to the right (west) of the section. The peak above the Mississippian on the regional synthetic traces corresponds to the Detrital member. Its reflection character changes greatly toward the location of the channel as it becomes replaced with the channel-fill sediments, and becomes seismically unresolvable from them at the channel. On the right side of the section, reflections contained in the Detrital formation can be seen to onlap the Mississippian. Above the Detrital, the Sunburst member (not interpreted in Figure 30) and Ostracod beds correspond to a trough, which narrows and increases in amplitude as they are replaced with the channel sediments towards the center of the section.

Above the Sunburst and Ostracod formations is a doublet peak that corresponds to the Coal 2 and Coal 3 formations, which ties to a doublet in the seismic data (only Coal 1 is interpreted in Figure 30, that ties to the overlying trough). Over the channel, the doublet turns into a single peak; this change in reflection character is possibly compaction related. For earlier times, the trace is the same as the channel synthetic due to log splicing.

To summarize the observations, the Glauconite channel appears as a high-amplitude trough surrounded (in time) by two single peaks. Towards the regional formations, the trough broadens out and decreases in amplitude slightly, and the positive amplitude peaks surrounding it turn into doublets. These results are similar to observations made by Miller *et al.* (1995), for a 2-D line that intersects the channel at a different location. They observed that the Glauconite trough tends to decrease in amplitude and become replaced by the Detrital peak off-channel. The comparison is complicated by the fact that the boundaries between different channel fills resolve seismically in the 1995 survey, which does not appear to be the case for the Blackfoot III survey. The coal markers may change their reflection character from a doublet to single peak due to a compaction relationship with the underlying Glauconite. Using these observations, the location of the channel is interpreted to be between CDP's 36 and 61.

Figure 31 shows the interpreted radial channel migrated sections from the surface geophones, with inserted P-S synthetic channel and regional traces, for the zone of interest. The quality of the tie appears to be slightly better than the vertical channel synthetic ties, and there is less trace stretching. The Glauconite channel corresponds to a peak at the end of the channel synthetic, which ties to a peak on the section. Above this is a broad trough, the bottom portion of which correlates to the coal markers.

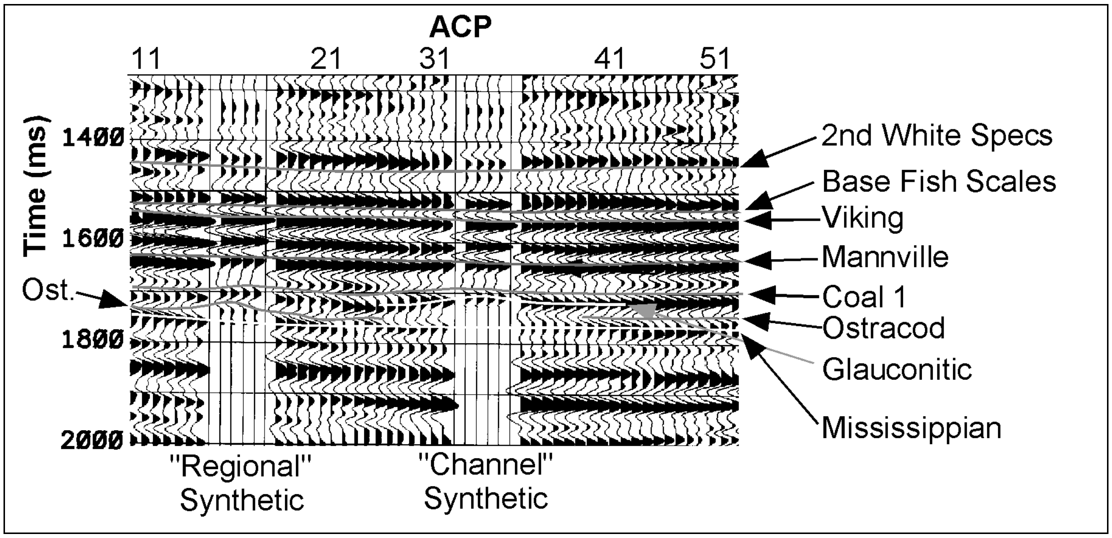

Figure 31. Channel and regional synthetic traces P-S synthetic traces spliced into radial channel data.

The peak at the end of the regional synthetic traces correlates to the Mississippian, but the Detrital peak above does not correlate to the data, making its interpretation uncertain. The Sunburst (not interpreted) and Ostracod formations correlate to a small trough above this, which broadens out towards channel as they become replaced by the channel-fill Glauconitic sediments. The first zero-crossing of the overlying peak corresponds to the coal markers, representing the splice point. In the seismic data, above the Coal 1 reflection there appears a small peak in a larger trough in the off-channel locations, which becomes a single broad trough above the channel. Again, this change in reflection character on- and off-channel may be due to differential compaction due to the underlying formations.

Mississippian and Deep Regional Synthetic Ties

An interpretation of the vertical channel data for reflectors both in and outside of the zone of interest appears in Figure 32. Reflections from the Mississippian and deeper were interpreted using synthetic traces from spliced well log data. The channel synthetic trace shows a strong peak at the very end corresponding to the Mississippian. There is no clear corresponding peak on the migrated section. The irregular surface of the Mississippian may be a factor in the mis-tie, as the 08-08 well is located over a kilometer away from the 09-08 well it has been spliced into. Differences in the reflection character of the Mississippian between the two locations may be too great to permit a clear tie.

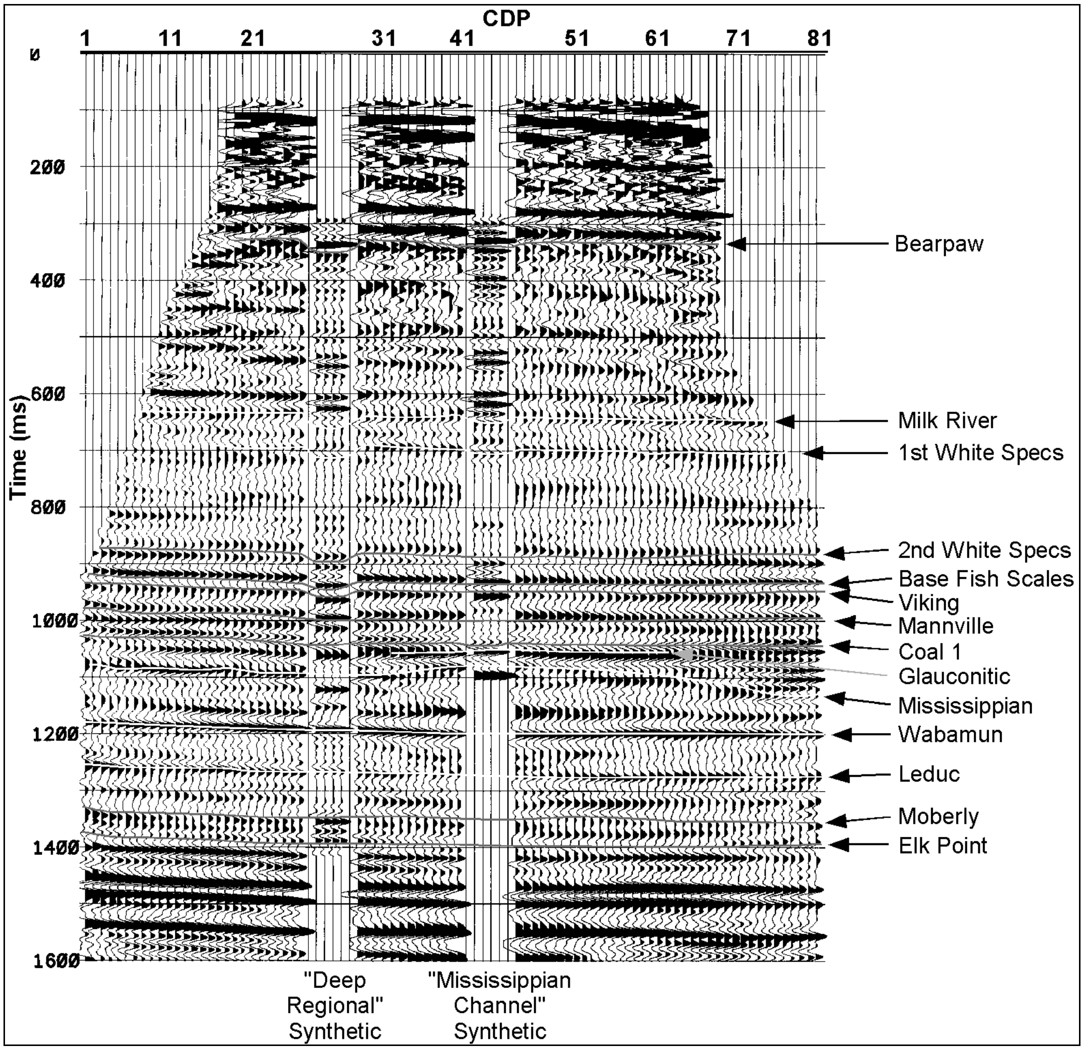

Figure 32. Channel and deep regional P-P synthetic ties to seismic data.

The deep regional synthetic traces are inserted where there is good correlation to reflections below the splice point. The high-quality agreement between the synthetic and migrated data results in a fairly unambiguous interpretation of reflections from the Banff formation and below. Above the splice point (Coal 3b), reflections are mis-tied by about 50 ms. This is because the 14-03 well was located on a Cambrian horst block, as shown in an earlier 3-D survey (Yang *et al*., 1996), whereas the Blackfoot III survey was not. The horst caused about 50 ms of time displacement for pre-Wabamun reflectors and even affected later formations. There is a poor tie to the data at the Mississippian. As before, this may be due to different reflection character and depth of the Mississippian between the well logs that were spliced to create the synthetic trace. There may be an additional noise factor of off-line energy scattering from the irregular surface of the Mississippian, which would obscure its in-line reflection.

Figure 33 shows the Mississippian Reflection and Deep Regional P-S synthetic traces inserted into the converted-wave migrated section. The section contains some edge effect migration artifacts at the extreme left and right, but has good quality for the central, high-fold portion. The Mississippian peak at the bottom of the

Contents

“Mississippian channel” synthetic correlates to a peak on the migrated data, while the trough and part of the next peak above it correlates to the Glauconite. The trough narrows to either side of the insertion point, possibly because the channel sediments are becoming replaced by the regional Detrial, Sunburst and Ostracod formations. These regional formations do not appear to resolve seismically.

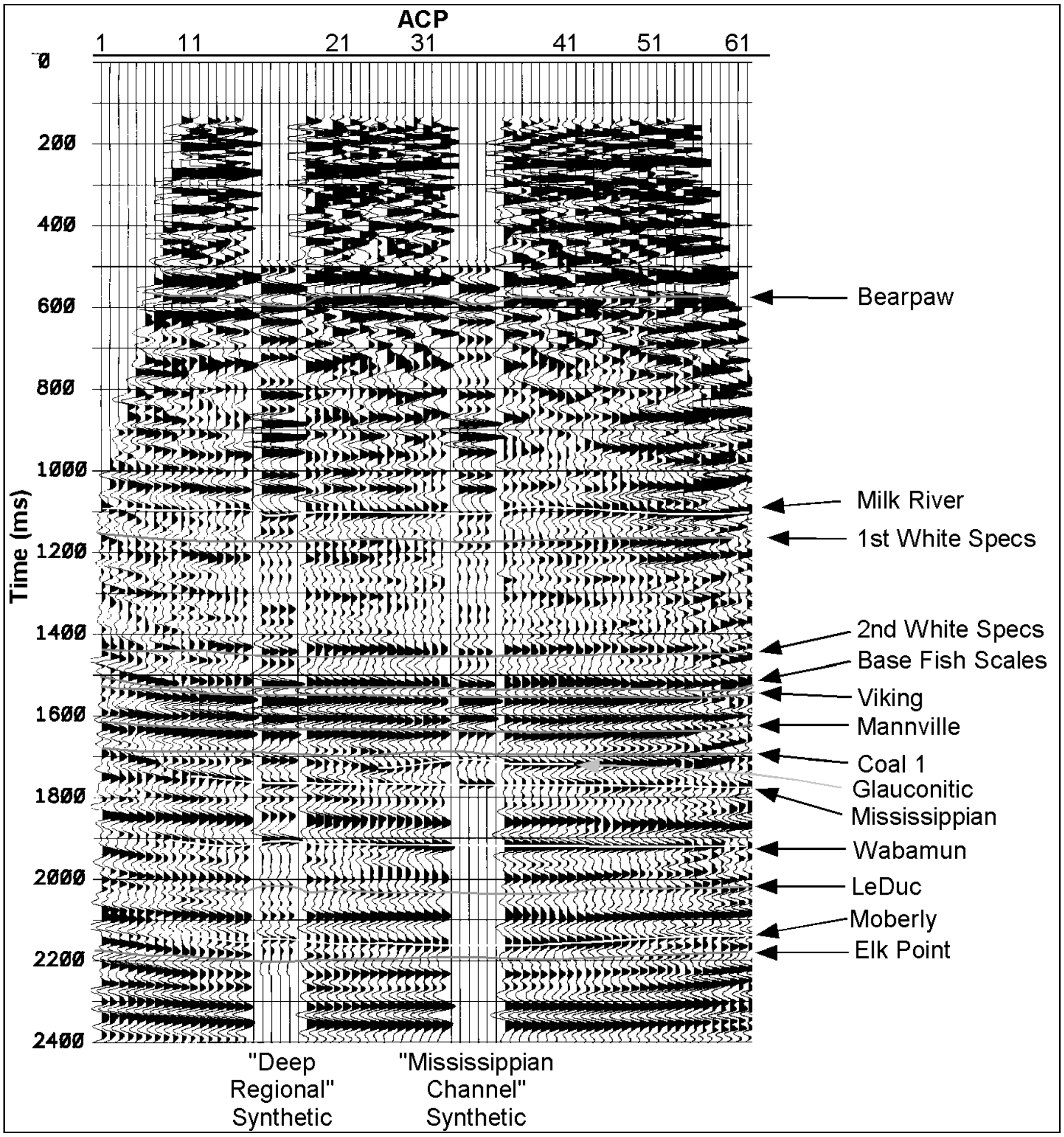

Figure 33. Channel and deep regional P-S synthetic ties to seismic data.

The Deep Regional synthetic has an excellent tie to the data for most of the trace length, with a minor amount of stretching for earlier reflections. For reasons not completely clear, the large mis-tie for earlier reflections seen in the vertical channel data is not present for the radial-channel data. It is possible that inaccuracies in assumed Vp/Vs are, coincidentally, cancelling out timing errors due to the Cambrian horst block. The Mississippian peak on the synthetic trace does tie to a peak on the seismic data, but given the large distance (>11 km) between spliced log and the surveyed data, and the complex surface of the Mississippian, this tie must be regarded with caution.

In general, the channel-fill sediments have a converted-wave seismic expression of a broad trough beneath a peak. Towards regional facies, the trough narrows, though the exact location of the channel edge is ambiguous. Formations above the Coal 1 marker change reflection character as they cross the channel, possibly due to differential compaction.

Largely due to superior data quality, the channel was more easily interpreted on the vertical than the radial sections.

CONCLUSIONS

The buried geophone data in general suffered from poorer data quality and less consistent bandwidth than the surface geophone data, likely as a result of mode leakage (caused by receiver misalignment) and inconsistent geophone coupling (caused by hole caving). Because of this, no attenuation was detected for the converted wave between the various geophone depths.

P-wave interval velocities indicate a thinning of the near-surface layer at the eastern third of the receiver line, which coincides with an increase in elevation. S-wave interval velocities are essentially unrelated to P-wave interval velocities and elevation. Velocities between buried geophone intervals were unphysically large for P-waves, perhaps as a result of insufficient P-wave refraction to vertical, or limitations of recording system time measurement.

Stack similarity computations show that random noise level is the chief determinant in the absolute similarity of buried geophone processed sections. Relative similarity is controlled primarily by the relative depth of sections and secondarily by their absolute depth. This relation is stronger for vertical channel sections than the radial channel sections, probably due to the high random noise levels in the latter. Sections from similar geophone depths tend to be similar as they may have a similar frequency notching pattern. Shallower data has higher raw reflection amplitude, and therefore higher signal-to-incoherent noise levels. This may cause shallower data to be more similar than deeper data.

On the vertical channel data, the Glauconite channel appears as a high-amplitude trough surrounded by two peaks. Off-channel, the trough broadens out, decreases in amplitude, and the peaks turn into doublets. The channel is also a broad trough on the converted-wave section that narrows slightly off-channel, making its interpretation more ambiguous than the P-P interpretation.

RECOMMENDATIONS

A shallow, multi-level VSP survey through the top 100 meters or so of the near surface may resolve the issue of where converted-wave bandwidth becomes attenuated between bedrock and surface. VSP surveys allow for more consistent coupling and greater control over geophone levelling and alignment than is possible for buried geophones. This shallow VSP survey could be done as an inexpensive add-on to a conventional, deep VSP survey.

ACKNOWLEDGMENTS

We would like to thank the sponsors of CREWES for their support in this research. The staff of CREWES provided invaluable assistance and support, for which we are grateful. Also, thanks to Dr. Gary Margrave for his helpful suggestions.

REFERENCES

Cary, P.W., and Eaton, D.W.D. A simple method for resolving large converted-wave (P-SV) statics. Geophysics **58**, p. 429-433.

Cieslewicz, D. and Lawton, D.C., 1997. A three-component field study of the effect of the low-velocity layer on converted-wave seismic data. CREWES Research Report **8**, Ch. 4.

DiSiena, J.P., Gaiser, J.E., and Corrigan, D., 1984. Horizontal components and shear wave analysis of three-component VSP data. In *Vertical Seismic Profiling, Part B: Advanced Concepts*. Toksöz and Stewart (eds.), Geophysical Press, p. 177-188.

Dufour, J., Squires, J., Edmunds, A, and Shook, I, 1998. Integrated geological and geophysical interpretation of the Blackfoot area, Southern Alberta. Canadian Society of Exploration Geophysicists Annual General Meeting, Technical Abstracts, p. 234-236.

Fromm, G., Krey, T., and Wiest, B., 1985. Static and dynamic corrections; in Dohr, G., Ed., Seismic Shear Waves: *Handbook of Geophysical Exploration* **15a**, Geophysical Press, 191-225.

Geis, W.T., Stewart, R.R., Jones, M.J., and Katopodis, P.E., 1990. Processing, correlating, and interpreting converted shear-waves from borehole data in southern Alberta: Geophysics, **55**, 660-669.

Kudo, K., and Shina, E., 1970. Attenuation of shear waves in soil. Bulletin of the Earthquake Research Institute **48**, p. 145-148.

Lawton, D.C., 1990. A 9-component refraction seismic experiment: Canadian Journal of Exploration Geophysics, **26**, 7-16.

Lawton, D.C. and Harrison, M.P., 1992. A two-component reflection seismic survey, Springbank, Alberta. Canadian Journal of Exploration Geophysics **28**, p. 30-43.

Larner, K., Chambers, R., Yand, M., Lynn, W. and Wai, W., 1983. Coherent noise in marine seismic data. Geophysics **48**, p. 854-886.

Margrave, G.F., 1998, unpublished. Seismic signal band estimation using f-x spectra.

Margrave, G.F., and Foltinek, D.S. 1995. Synthetic P-P and P-SV cross sections. CREWES Research Report **7**, Ch. 5.

Miller, S.L.M., Aydemir, E.O., and Margrave, G.F., 1995. Preliminary interpretation of P-P and P-S seismic data from the Blackfoot broad-band survey. CREWES Research Report **7**, Ch. 42.

Porter-Hirsche, J. and Hirsche, K., 1998. Repeatability study of land data acquisition and processing for time lapse seismic. Society of Exploration Geophysicists 68th Annual General Meeting Technical Abstracts, p. 9-11.

Sheriff, R.E. and Geldart, L.P., 1995. *Exploration Seismology*, 2nd ed. Cambridge University Press, Cambridge.

Simin, V., Harrison, M.P., and Lorentz, G.A., 1996. Processing the Blackfoot 3C-3D seismic survey. CREWES Research Report **8**, Ch. 39.

Stewart, R.R., Huddleston, P.D., and Kan, T.K., 1984. Seismic versus sonic velocities: A vertical seismic profiling study. Geophysics **49**, p. 1153-1168.

Toksöz, M.N, Johnston, D.H., and Timur, A., 1979. Attenuation of seismic waves in dry and saturated rocks: I. Laboratory measurements. Geophysics, **44**, 681-690.

Yang, Y.C.G., Lawton, D.C., Stewart, R.R., Miller, S.L.M., Potter, C.C., and Simin, V. 1996. Interpretation and analysis of the Blackfoot 3C-3D seismic survey. CREWES Research Report **8**, Ch. 46.

Zhang, Q., San, Z., Brown, R.J. and Stewart, R.R., 1994. VSP interpretation from Joffre, Alberta. CREWES Research Report **6**, Ch. 33.